8-3-2017

Computational Insights into Enzymatic Ring Opening Mechanisms

Travis Michael DeWolfe
University of Windsor

Computational Insights into Enzymatic Ring Opening Mechanisms

By

Travis DeWolfe

A Thesis

Submitted to the Faculty of Graduate Studies

through the Department of Chemistry and Biochemistry

in Partial Fulfillment of the Requirements for

the Degree of Master of Science

at the University of Windsor

Windsor, Ontario, Canada

2017

Computational Insights into Enzymatic Ring Opening Mechanisms

by

Travis DeWolfe

APPROVED BY:

_____

L. Porter
Department of Biological Sciences

_____

P. Vacratsis
Department of Chemistry & Biochemistry

_____

J. Gauld, Advisor
Department of Chemistry & Biochemistry

June 13, 2017

Declaration of Co-Authorship

I hereby declare that this thesis incorporates material that is a result of joint research as follows:

Chapter 4: was done in collaboration with Wanlei Wei under the supervision of Prof. James W. Gauld.

In all cases, the key ideas, primary contributions, experimental designs, data analysis, interpretation, and writing were performed by the author, and the contribution of the co-authors was primarily through the provision of Wanlei Wei performing the molecular dynamic simulations; Prof. James W. Gauld provided feedback, guidance, and refinement of ideas.

I am aware of the University of Windsor Senate Policy on Authorship and I certify that I have properly acknowledged the contribution of other researchers to my thesis, and have obtained written permission from each of the co-author(s) to include the above material in my thesis.

I certify that, with the above qualifications, this thesis, and the research it refers, is the product of my own work.

I certify that the above material describes work completed during my registration as graduate student at the University of Windsor.

I declare that, to the best of my knowledge, my dissertation does not infringe upon anyone's copyright nor violate any proprietary rights and that any ideas, techniques, quotations, or any other material from the work of other people included in my dissertation, published or otherwise, are fully acknowledged in accordance with the standard referencing practices. Furthermore, to the extent that I have included copyrighted material that surpasses the bounds of fair dealing within the meaning of the Canada Copyright Act, I certify that I have obtained a written permission from the copyright owners to include such materials in my dissertation.

I declare that this is a true copy of my dissertation, including any final revisions, as approved by my dissertation committee and the Graduate Studies office, and that this dissertation has not been submitted for a higher degree to any other University or Institution.

Abstract

Using a range of computational chemistry methods including Molecular Dynamics (MD) simulations, quantum mechanical (QM)-chemical cluster, and quantum mechanics/molecular mechanics (QM/M) methods, we have investigated the catalytic mechanism and inhibition of two physiologically important enzymes; glucosamine-6-phosphate synthase and CTX-M β-lactamase, respectively.

More specifically, for the inhibition of CTX-M β-lactamase it was observed that an active site serinyl (Ser130) residue initially assists in stabilizing the reactive complex. The side-chain hydroxyl (β-OH) of Ser130 is deprotonated by the nearby side-chain amine of Lys73. This enables the resulting now oxyanionic β-oxygen to nucleophilically attack the substrate's key ring carbonyl carbon centre. This reaction step occurs with a barrier of 74.5 kJ mol^{-1} and results in the formation of a covalently cross-linked enzyme-ligand intermediate. Interestingly, whether Lys73 is initially in its protonated or neutral state in the reactive complex, due to the nearby presence of a glutamate residue, it is able to readily act as a base to deprotonate the side-chain hydroxyl of Ser130.

For glucosamine-6-phosphate synthase, the protonation state of His504 and its catalytic role were elucidated. The mechanism for opening of the substrate's sugar ring in which His504 initially acts as an acid but later as a base, occurs with a barrier of 107.2 kJ mol^{-1}. An alternative pathway was considered in which Glu488 is able to act as a base and His504 as an acid. This mechanism was found to occur with a lower reaction barrier of 91.5 kJ mol^{-1}. The results of MD simulations also supported the suggesting of His504 being protonated as it results in a more consistent active site-bound reactive complex. The work in this thesis highlight the significance of approaching enzymatic systems through both molecular dynamic and quantum mechanical/molecular mechanical techniques.

Dedication

I dedicate this work to my family and friends.

Acknowledgements

I would like to thank Dr. James Gauld for the opportunity to conduct research in his lab for both my graduate degree and my undergraduate thesis. Your advice and mentorship has been very valuable over the years. I would like to thank my undergraduate mentor and friend, Dr. Mohamed Aboelgna. I will never forget the powerful friendship and mentorship you have given me. It has been an absolute pleasure working with you for the past 3 years. I wish you all the best in your post-doc adventures!

I would also like to thank all the past and current members of the Gauld Group. You have all been extremely helpful and entertaining throughout the years. Sameer, you have been an amazing friend and although our conversations had gotten a little out of hand I wouldn't have changed a thing. I am glad I was able to gain a great, tremendous friendship out of this experience. Trust me, I know friendships and friendships know me, and I can say that this friendship is the best. Really. Just the best. Tremendous friendship. Good guy, let me tell you.

Thank you to Dr. John Hayward for your advice throughout my last year here and the chemical knowledge you have shared. I wish you all the best in your future career and if you are instructing general chemistry next year, please try to one-up our last demonstration. Paul, it has been fun having the opportunity to GA with you, thank you for your advice. Stay positive and powerful.

I would also like to thank my readers, Dr. Porter and Dr. Vacratsis. Thank you for taking the time out of your busy schedules to read my thesis and be a part of my committee.

Lastly, and most importantly, my boo. My ride or die. My moon and stars. And all the other ridiculous, sappy, ghetto, sweet things we call each other. I wouldn't be

here if it wasn't for you. You have taught me so much about myself; this thesis is as much yours as it is mine. You have held me steady and had my back through the hardest times. You have encouraged me to push myself and stay true. All the stress and the late nights are coming to an end. This is the end of the beginning and I look forward to living my life with you. I love you. Now hurry up and finish your BScN, you got a lot of catching up to do!

Table of Contents

Declaration of Co-Authorship iii
Abstract v
Dedication vi
Acknowledgements vii
List of Figures xii
List of Schemes xv
List of Abbreviations and Symbols xvi
Chapter 1: Introduction 1
1.1 Introduction 2
1.2 Understanding Enzyme Catalysis 3
1.3 Antibiotic Resistance and β-lactamase Inhibition 5
1.4 The Synthetic Domain of Glucosamine 6-P Synthase 6
1.5 Application of Computational Chemistry to Enzymatic Processes 6
1.6 References 8
Chapter 2: Computational Approaches to Enzymology 11
2.1 Introduction 12
2.2 Quantum Mechanics 12
2.3 Molecular Mechanics 14
2.4 Molecular Dynamic Simulations and Enzymes 16
2.5 Quantum Mechanical Clusters and Proton Affinities 17
2.6 Quantum Mechanic/Molecular Mechanic Models 18
2.7 Software 22
2.8 References 23
Chapter 3: The Inhibition Mechanism of CTX-M β-Lactamases 28
3.1 Introduction 29
3.2 Computational Details 33

3.2.1 Molecular Docking 33
3.2.2 Molecular Dynamics 33
3.2.3 QM/MM Calculations 34
3.3 Results and Discussion 34
3.3.1 The Reactive Complex 34
3.3.1.1 The Reactive Complex with Protonated Lys73 37
3.3.1.2 The Reactive Complex with Neutral Lys73 39
3.3.2 The Formation of the Bridging Intermediate 40
3.4 Conclusion 44
3.5 References 45
Chapter 4: Ring Opening Mechanism of Glucosamine-6-Phosphate Synthase 50
4.1 Introduction 51
4.2 Computational Details 53
4.2.1 Sample Preparation 53
4.2.2 Molecular Dynamics 54
4.2.3 QM/MM Calculations 55
4.3 Results And Discussion 56
4.3.1 The Protonation State of His504's Imidazole 56
4.3.2 The Ring Opening Mechanism Initiated by His504 61
4.3.3 The Ring Opening Mechanism Initiated by Glu488 63
4.4 Conclusion 66
4.5 References 68
Chapter 5: Conclusions 74
5.1 Conclusions 75
5.2 References 77
Chapter 6: Future Work 78
6.1 Future Work 79
6.2 References 81

Vita Auctoris 82

List of Figures

Figure 1.1. Schematic representation of the three blood type sugar antigens, A, B and O. 2

Figure 1.2. Reaction coordinate diagram showcasing an uncatalyzed reaction (red) versus an enzyme catalyzed reaction (green). 4

Figure 1.2 Various core lactam ring structures; A) oxacephem, B) carbacephem, C) carbapenam, D) penem, and E) oxapenam..... 5

Figure 2.1 A ball and stick representation of the various forces calculated by molecular mechanics. 15

Figure 2.2 An example of a QM/MM model, the MM region is represented by the wireframe structure, the QM region is represented as ball and sticks. 19

Figure 2.3 A representative illustration of the two coupling schemes for QM/MM models, additive and subtractive. 20

Figure 3.1. The chemical structure of the FDA approved β-lactamases inhibitors…30

Figure 3.2. Overlays of structures obtained from cluster analysis of RMSD produced from 10ns production run of the reactive complex (A) Lys73 in its protonated state and (B) Lys73 in its neutral state. 35

Figure 3.3. A distance plot of $_{Lys73}N\cdots O_{Ser130}$ over a 10ns production run of the reactive complex with (A) Lys73's protonated state and (B) Lys73's neutral state..36

Figure 3.4. Overlay structures (A) obtained from cluster analysis of RMSD (B) produced from 10ns production run on the reactive complex of S130G variant.....36

Figure 3.5. A distance plot produced from a 10ns production run on of the reaction complex of (A) Lys73 in its protonated state, (B) Lys73 in its neutral state, and (C) the S130G variant. 37

Figure 3.6. Relative energy surface obtained for the covalent formation of Ser70 to tazobactam, with Lys73 protonated and Glu166 deprotonated in **$RC_{(Lys\text{-}H+)}$**. See Computational Details.....38

Figure 3.7. Relative energy surface obtained for the covalent formation of Ser70 to tazobactam, with Lys73 neutral and Glu166 neutral in **$RC_{(Lys\text{-}Neu)}$**. See Computational Details.....39

Figure 3.8. Overlay of structures (A) obtained from cluster analysis of RMSD produced from 4ns production run of the intermediate complex with Lys73 neutral. Distance plot (B) of Ser130's oxygen to tazobactam's carbon generated from 4ns production run with Lys73 neutral.....41

Figure 3.9. Overlay of structures obtained from cluster analysis of RMSD produced from 4ns production run of the intermediate complex with Lys73 protonated.....41

Figure 3.10. Overlay structures (A) obtained from cluster analysis of RMSD (B) produced from 4ns production run on the intermediate complex of S130G variant. 42

Figure 3.11. Relative energy surface obtained for the covalent formation of Ser130 to tazobactam intermediate, see Computational Details.....43

Figure 4.1. A RMSD plot of all atoms within ~12 Å of Fru-6-P relative to their crystal structure over a 100ns production run with His504 protonated in blue and His504 neutral in orange.....56

Figure 4.2. A distance plot of $_{His504}N\cdots O_{Fru\text{-}6\text{-}P}$ over a 100ns production run with His504 protonated in blue and His504 neutral in orange. The chart on the right shows the occurrence of each distance as a percentage.....57

Figure 4.3. Representative structures selected from a 100 ns production run (see Computational Details) with His504 (A) protonated and (B) neutral, distances in Ångstrom. Ligand interaction diagrams showcasing percentage of interactions over the simulation are also shown for the His504 (C) protonated and (D) neutral.....58

Figure 4.4. A distance plot of $_{His504}N\cdots HO\text{-}_{Fru\text{-}6\text{-}P}$ over a 100ns production run with His504 neutral. 59

Figure 4.5. Calculated proton affinities of His504's imidazole and Glu488's carboxyl compared to their molecular equivalents. The calculated proton affinity of water is 745.6 kJ mol^{-1}. 60

Figure 4.6. Optimized structures of the reactant complex (**$RC_{(His)}$**), intermediates (**$IM_{(His)}$**), and transition structures (**$TS_{(His)}$**) of the ring opening mechanism catalyzed by His504, highlighting key residues and relevant distances in Ångstrom. 61

Figure 4.7. Potential energy surface obtained for the ring opening mechanism catalyzed by His504, see Computational Details. 62

Figure 4.8. Optimized structures of the reactant complex (**$RC_{(His/Glu)}$**), intermediates (**$IM_{(His/Glu)}$**), and transition structures (**$TS_{(His/Glu)}$**) of the ring opening mechanism catalyzed by Glu488 and His504, highlighting key residues and relevant distances in Ångstrom. 64

Figure 4.9. Potential energy surface obtained for the ring opening mechanism catalyzed by Glu488 and His504, see Computational Details. 65

List of Schemes

Scheme 1.1 Reaction of glucosamine-6-phosphate synthase. 6

Scheme 3.1. Reaction pathway of β-lactam antibiotic hydrolysis. 29

Scheme 3.2. Reaction pathway of cross-linked species formation with tazobactam.[24] 32

Scheme 4.1. Proposed reaction for fructose-6-phosphate ring opening catalyzed by GlmS.[18] 53

Scheme 6.1. Proposed reaction pathway of cross-linked species formation with tazobactam with (A) sulfinate acting as the acid/base catalyst and (B) carboxylate acting as the acid/base catalyst. 79

List of Abbreviations and Symbols

Abbreviations

AMBER	Assisted Model Building with Energy Refinement (force field and/or MD program)
DFT	Density functional theory
(R)ESP	(Restrained) Electrostatic potential
Fru-6-P	Fructose-6-phosphate
GlmS	Glucosamine-6-phosphate synthase
GFA	Glutamine:fructose-6-phosphate amidotransferase
GlcN-6-P	Glucosamine-6-phoshpate
HF	Hartree-Fock
IC	Intermediate Complex
MD	Molecular Dynamics
MM	Molecular Mechanics
MOE	Molecular Operating Environment (program)
NAMD	Nanoscale molecular dynamics
ONIOM	Our own n-layered integrated molecular orbital and molecular mechanics

PA	Proton affinity
PC	Product complex
PDB	Protein Data Bank
QM	Quantum Mechanics
QM/MM	Quantum Mechanics/Molecular Mechanics
RC	Reactant Complex
RMSD	Root-mean square deviation
TS	Transition state
UDP-N-acetylglucosamine	Uridine diphosphate N-acetylglucosamine
VMD	Visual Molecular Dynamics

Units symbols

Å	Angstroms
kJ mol^{-1}	Kilojoules per mole

Chapter 1:
Introduction

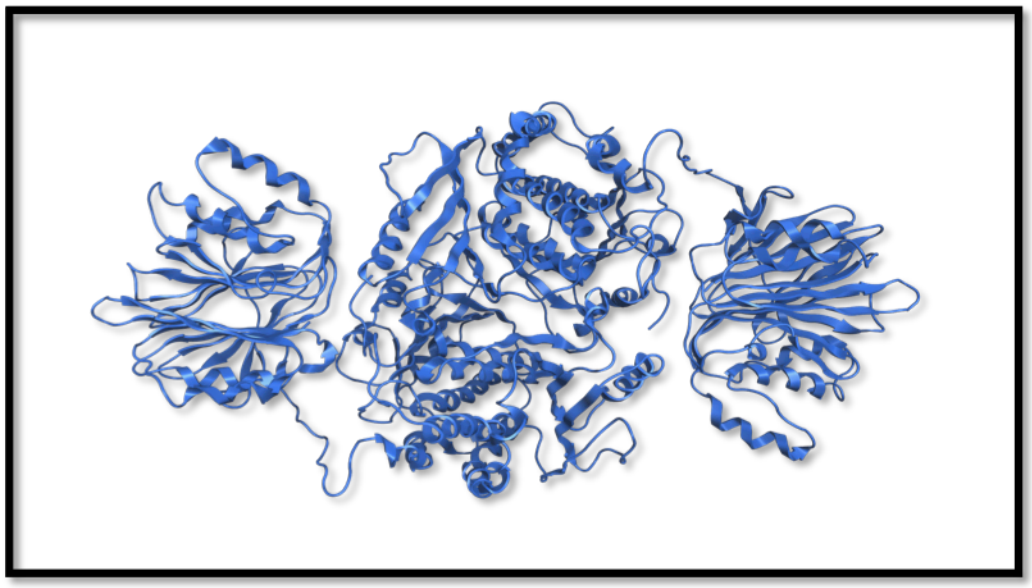

1.1 Introduction

Heterocyclic ring systems are ubiquitous chemical features found across the spectrum of biologically relevant molecules. A wide variety of synthetic and natural ring-containing compounds found throughout biochemistry are integral to biochemical and physiological systems. The well-defined geometry of functional groups around a ring system has a significant impact on the structures and functions of the biomolecules. For example different sugar systems often vary by only a single atom or two, or a small difference in geometry, which can have substantial effects on their physical and (bio)chemical properties.[1-3] Fructose and glucose are both hexoses, having the formula $C_6H_{12}O$, but fructose is a five-membered ring sugar while glucose is a six membered ring.[2] The latter has a lower solubility in water. Another example can be found in the blood cell antigens, which are composed of a variety of sugar rings (Figure 1.1).[1] Mixing of the wrong blood types can lead to a dangerous and rapid immune response, arising from the slight variance in sugar ring systems of the antigens.

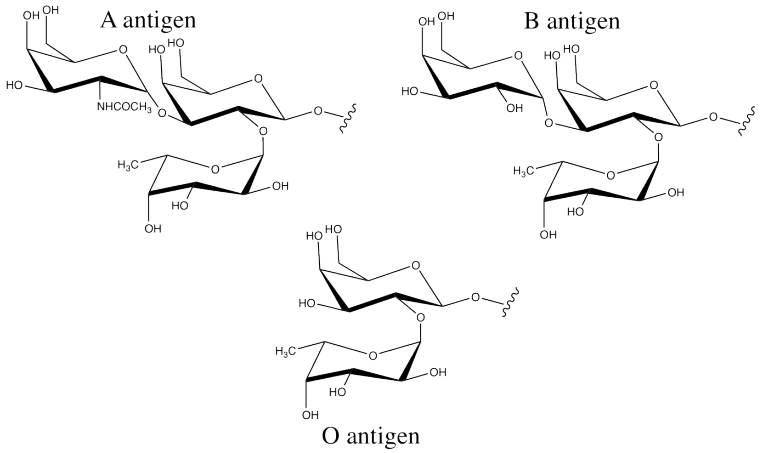

Figure 1.1. Schematic representation of the three blood type sugar antigens, A, B and O.

Another vitally important class of ring system are those containing nitrogen. This includes a wide spectrum of biologically relevant molecules such as nucleic acids, amino acid metabolites, and pharmaceuticals. For example, one must not understate the significant effects nicotine, a nitrogen-containing heterocyclic compound, has on the parasympathetic nervous system of the human body.[4] Of course, this is not limited to naturally-occurring compounds. Synthetic compounds, such as barbiturates, also have potent effects.[5] These are central nervous system depressants capable of producing anesthetic effects for several hours. We cannot underappreciate the diverse capabilities of ring systems in biological systems. It is therefore important to deepen our understanding of these diverse, robust compounds and their relation to enzymatic systems.

1.2 Understanding Enzyme Catalysis

Enzymes are remarkable biocatalysts that are essential for life. They are composed from a set of 20 genetically encoded amino acids, some of which may be post-translationally modified, linked together with amide bonds to form polypeptides. Some also incorporate non-protein molecules such as cofactors or metals. This provides them with a great diversity in structure and chemical functionality, and as a result they are able to catalyze the variety of physiologically important reactions that range from simple proton transfers to the hydrolysis and break-down of complex molecules.[6] Comprehending how their rate enhancements are achieved remains one of the most crucial steps in understanding biological catalysis. It is important to explore the intricacies of their reactions to exploit or inhibit the reactions of these impressive biological catalysts.[7]

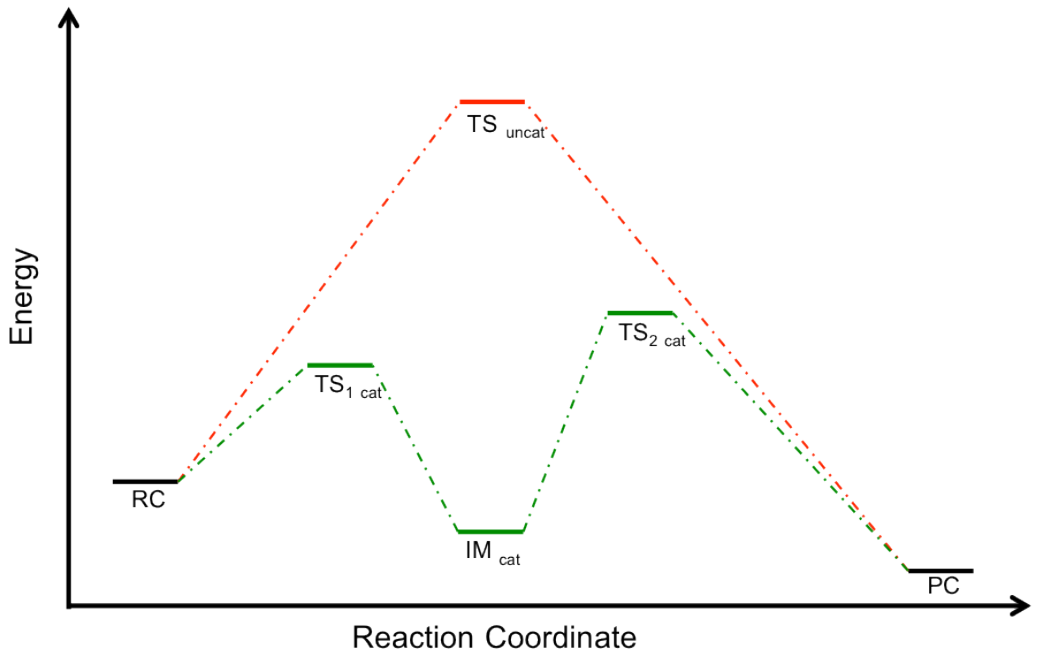

Figure 1.2. Reaction coordinate diagram showcasing an uncatalyzed reaction (red) versus an enzyme catalyzed reaction (green).

Enzymes are able to achieve their rate enhancement capabilities through a variety of different chemical strategies.[8] The major contributing factor is the lowering of the activation energy of the reaction through the stabilization of the high-energy transition states that occur (Figure 1.2).[9] A variety of factors can contribute to this stabilization, such as the electrostatic environment or a hydrogen bonding network within the active site.[10] Enzymes also provide an environment for proximity. The active site exists as a microenvironment that places the substrates in a geometry that is extremely favourable for the reaction to occur.[9,11] Other factors that affect enzyme catalysis may include quantum tunneling, conformational dynamics, and desolvation.[8] Most importantly, while one factor may contribute more than another, it is often a combination of these effects that drive the process of catalysis.

1.3 Antibiotic Resistance and β-lactamase Inhibition

Unfortunately, our species is on the verge of losing some of our most recent medical advancements thanks to the rise of antibiotic resistant bacteria.[12] Indeed, overuse of common antibiotics has led to the emergence of bacteria capable of surviving our strongest antibiotics.[13] While antibiotic resistance is the cumulative result of a variety of systems, one particular culprit is the enzyme β-lactamase.[14]

The discovery of penicillin and its application to treating bacterial infections has had a monumental effect on human and animal health in the last century. This discovery led to the creation of β-lactam antibiotics, bicyclic nitrogen-containing compounds (Figure 1.2).[15] These compounds directly inhibit the biosynthesis of peptidoglycan, which is used to make bacterial cell walls, and thus result in their death. Unfortunately, some bacteria contain β-lactamase, which hydrolytically opens the lactam ring, therefore making them inactive. One strategy to prevent this is to combine antibiotics with a β-lactamase inhibitor.[15] Understanding how β-lactamase is inhibited may create future leads for inhibitor design.

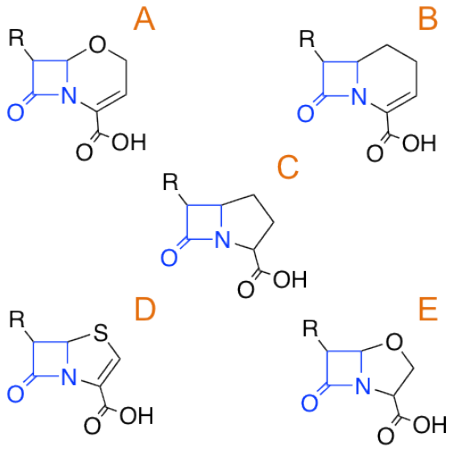

Figure 1.2 Various core lactam ring structures; A) oxacephem, B) carbacephem, C) carbapenam, D) penem, and E) oxapenam.

1.4 The Synthetic Domain of Glucosamine 6-P Synthase

Glucosamine 6-phosphate synthase is a multi-active site enzyme that belongs to the family of enzymes known as amidotransferases. This class of enzymes is responsible for deamination of glutamine to form glutamate and an aminated product.[16] In glucosamine-6-phosphate synthase's case, the overall reaction produces glucosamine-6-phosphate from the fructose-6-phosphate substrate (Scheme 1.1).[17] This produces glucosamine-6-phosphate, a crucial molecule used in a variety of biologically essential processes across a spectrum of organisms.

Scheme 1.1 Reaction of glucosamine-6-phosphate synthase.

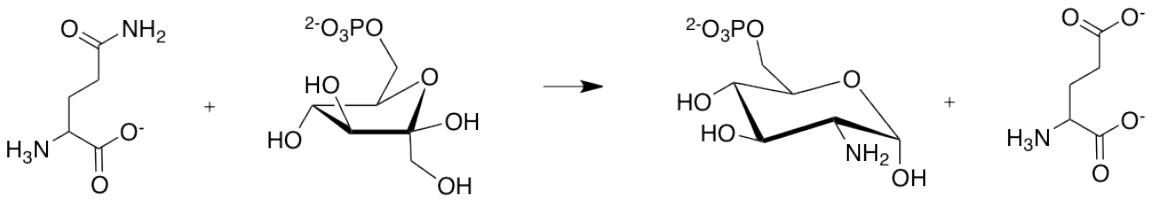

Deamination of glutamine occurs in the deaminase site, the ammonium ion produced then travels through an ~18 Å tunnel where it arrives at the synthase site.[18] This site is capable of two reactions; the ring opening of fructose-6-phosphate, and its amination to glucosamine-6-phosphate. Understanding the catalytic reaction of this enzyme is vital as its product has implications in diabetes, fungal chitin production, and bacteria's cell wall production.[19-21]

1.5 Application of Computational Chemistry to Enzymatic Processes

One of the most difficult challenges in studying enzymatic reactions arises from their high rate enhancement. It is extremely difficult to study the nuances of their

behaviour. For example, the decarboxylation reaction of orotidine 5'-phosphate takes 78 million years to occur, but with the help of the decarboxylase enzyme it is accomplished in less than a second.[22] Computational chemistry can allow us to circumvent this incredible speed of reaction. Indeed, computational chemistry has been shown to be a successful tool in studying these diverse catalysts by identifying difficult-to-characterize intermediates, transition states, and products along their reaction path.[23-25] The success of the computational enzymology approach was recognized in 2013 with a Nobel Prize.[26] The work in thesis explored the inhibition of CTX-M β-lactamase with tazobactam, with the objective of elucidating the mechanism of a bridged intermediate formation between Ser70 and Ser130. The synthetic site of glucosamine-6-phosphate was also investigated to gain atomistic insight into the ring opening mechanism of fructose-6-phosphate. In the subsequent chapter, we will delve into how computational chemistry is applied to exploring enzymatic catalysis.

1.6 References

(1) Watkins, W. M. The ABO blood group system: historical background. *Transfus. Med.* **2001**, *11*, 243.

(2) Rippe, J. M.; Angelopoulos, T. J. Sucrose, High-Fructose Corn Syrup, and Fructose, Their Metabolism and Potential Health Effects: What Do We Really Know? *Adv. Nutr.* **2013**, *4*, 236.

(3) Elliott, S. S.; Keim, N. L.; Stern, J. S.; Teff, K.; Havel, P. J. Fructose, weight gain, and the insulin resistance syndrome. *Am. J. Clin. Nutr.* **2002**, *76*, 911.

(4) Le Houezec, J. Role of nicotine pharmacokinetics and nicotine addiction and nicotine replacement therapy: a review. *Int. J. Tuberc. Lung. D.* **2003**, *7*, 811.

(5) Nicoll, R. A.; Eccles, J. C.; Oshima, T.; Rubia, F. Prolongation of Hippocampal Inhibitory Postsynaptic Potentials by Barbiturates. *Nature* **1975**, *258*, 625.

(6) Bugg, T. An Introduction to Enzyme and Coenzyme Chemistry; Blackwell Science: Oxford ; Cambridge, Mass., USA, 2000.

(7) Hilvert, D. Design of Protein Catalysts. *Annu. Rev. Biochem.* **2013**, *82*, 447.

(8) Llano, J.; Gauld, J. W. Chapter 23 Mechanistics of Enzyme Catalysis: From Small to Large Active‐Site Models; Wiler-VCH: Weinheim, 2010; Vol. 2.

(9) Benkovic, S. J.; Hammes-Schiffer, S. A perspective on enzyme catalysis. *Science* **2003**, *301*, 1196.

(10) Pauling, L. Molecular Architecture *Biolog. Sci.* **1946**, *24*, 1375.

(11) Cannon, W. R.; Singleton, S. F.; Benkovic, S. J. A perspective on biological catalysis. *Nat. Struct. Biol.* **1996**, *3*, 821.

(12) Neu, H. C. The Crisis in Antibiotic-Resistance. *Science* **1992**, *257*, 1064.

(13) Rodriguez-Rojas, A.; Rodriguez-Beltran, J.; Couce, A.; Blazquez, J. Antibiotics and antibiotic resistance: A bitter fight against evolution. *Int. J. Med. Microbiol.* **2013**, *303*, 293.

(14) Rossolini, G. M.; Arena, F.; Pecile, P.; Pollini, S. Update on the antibiotic resistance crisis. *Curr. Opin. Pharmacol.* **2014**, *18*, 56.

(15) Drawz, S. M.; Bonomo, R. A. Three Decades of beta-Lactamase Inhibitors. *Clin. Microbiol. Rev.* **2010**, *23*, 160.

(16) Massiere, F.; Badet-Denisot, M. A. The mechanism of glutamine-dependent amidotransferases. *Cell Mol. Life Sci.* **1998**, *54*, 205.

(17) Ghosh, S.; Blumenthal, H. J.; Davidson, E.; Roseman, S. Glucosamine metabolism. V. Enzymatic synthesis of glucosamine 6-phosphate. *J. Biol. Chem.* **1960**, *235*, 1265.

(18) Teplyakov, A.; Obmolova, G.; Badet, B.; Badet-Denisot, M. A. Channeling of ammonia in glucosamine-6-phosphate synthase. *J. Mol. Biol.* **2001**, *313*, 1093.

(19) Wojciechowski, M.; Milewski, S.; Mazerski, J.; Borowski, E. Glucosamine-6-phosphate synthase, a novel target for antifungal agents. Molecular modelling studies in drug design. *Acta. Biochim. Pol.* **2005**, *52*, 647.

(20) Moraes, G. L.; Gomes, G. C.; de Sousa, P. R. M.; Alves, C. N.; Govender, T.; Kruger, H. G.; Maguire, G. E. M.; Lamichhane, G.; Lameira, J. Structural and functional features of enzymes of Mycobacterium tuberculosis peptidoglycan biosynthesis as targets for drug development. *Tuberculosis* **2015**, *95*, 95.

(21) Kaneto, H.; Xu, G.; Song, K. H.; Suzuma, K.; Bonner-Weir, S.; Sharma, A.; Weir, G. C. Activation of the hexosamine pathway leads to deterioration of pancreatic beta-cell function through the induction of oxidative stress. *J. Biol. Chem.* **2001**, *276*, 31099.

(22) Radzicka, A.; Wolfenden, R. A Proficient Enzyme. *Science* **1995**, *267*, 90.

(23) Gherib, R.; Dokainish, H. M.; Gauld, J. W. Multi-scale computational enzymology: enhancing our understanding of enzymatic catalysis. *Int. J. Mol. Sci.* **2014**, *15*, 401.

(24) Pinto, G. P.; Bras, N. F.; Perez, M. A. S.; Fernandes, P. A.; Russo, N.; Ramos, M. J.; Toscano, M. Establishing the Catalytic Mechanism of Human Pancreatic alpha-Amylase with QM/MM Methods. *J. Chem. Theory Comput.* **2015**, *11*, 2508.

(25) Zhao, Y.; Chen, N.; Wu, R.; Cao, Z. A QM/MM MD study of the pH-dependent ring-opening catalysis and lid motif flexibility in glucosamine 6-phosphate deaminase. *Phys. Chem. Chem. Phys.* **2014**, *16*, 18406.

(26) Thiel, W.; Hummer, G. Nobel 2013 Chemistry: Methods for computational chemistry. *Nature* **2013**, *504*, 96.

Chapter 2: Computational Approaches to Enzymology

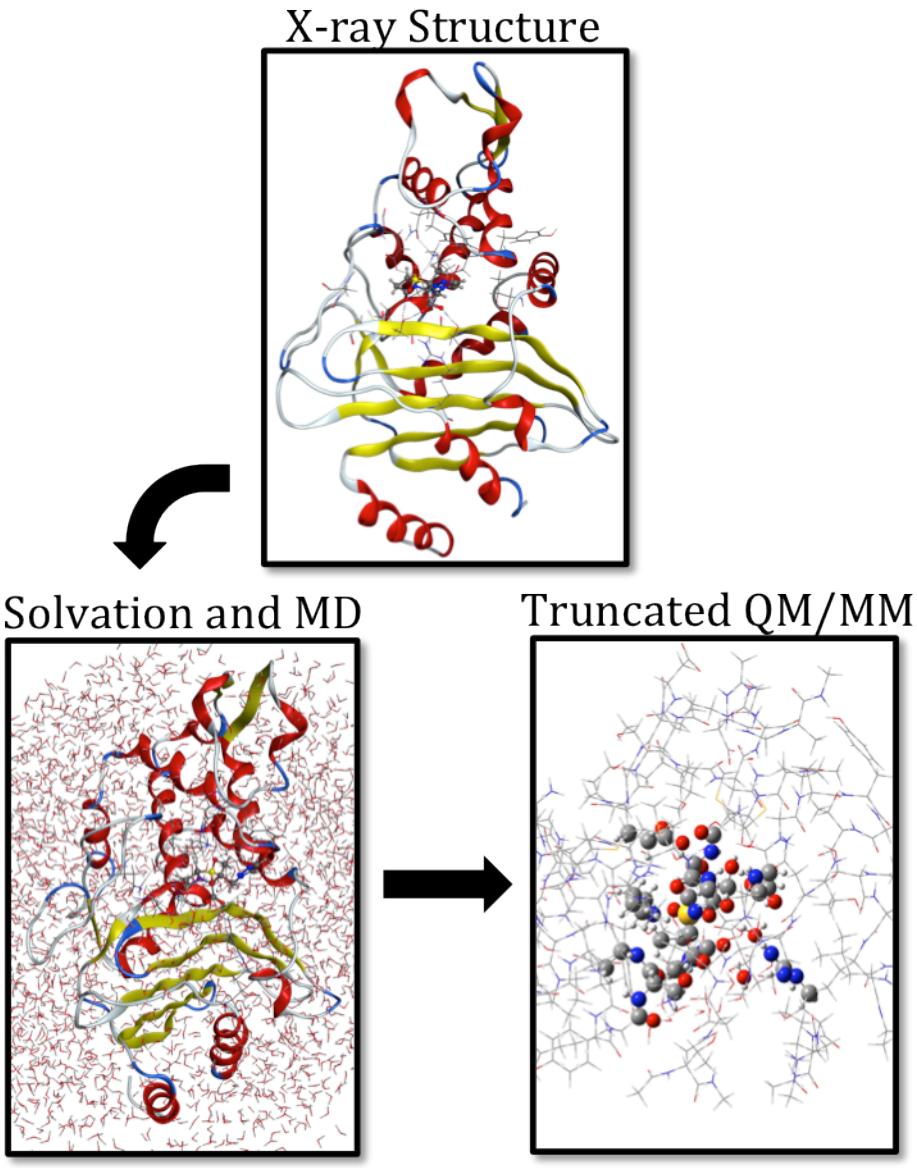

2.1 Introduction

For centuries our species believed the world was governed by conventional physics, that is Newton's Laws. As time progressed we discovered a world beyond what is visible to the naked eye, a quantum world of electrons, nuclei, protons, and various other quantum particles. We realized our previous laws of physics did not apply to this world and thus a new branch of physics was born; quantum physics. Computational chemists use this knowledge of the quantum world combined with the processing power of supercomputers to analyze chemical systems.[1] This has given an opportunity to provide significant insight into a variety of different chemical phenomena.

Herein, this chapter details what led to the development of this powerful tool and the methodologies applied to the subsequent computational enzymology studies. The methodology of molecular mechanics and dynamics will be outlined.

2.2 Quantum Mechanics

The foundational equation of all methods used in this thesis is Schrodinger's Equation.[2] In it is the wavefunction, which can provide all information of a chemical system. The time independent Schrodinger Equation is shown in Equation 2.1:

$$\hat{H}\psi = E\psi \qquad \textbf{Eq 2.1}$$

It contains the term E, which is the energy of the system describe by the wavefunction, and the Hamiltonian ($\hat{H}$). The Hamiltonian can be expanded as a sum of its kinetic and potential energies as shown in Equation 2.2:

$$\hat{H} = \hat{T} + \hat{V} \qquad \textbf{Eq 2.2}$$

These terms can be expanded to various components based on the type of interactions as shown in Equation 2.3:

$$\hat{H} = \hat{T}_n + \hat{T}_e + \hat{V}_{nn} + \hat{V}_{ne} + \hat{V}_{ee} \qquad \textbf{Eq 2.3}$$

Here we have five terms, both $\hat{T}_n$ and $\hat{T}_e$ are the kinetic energy operators of both nuclei and electrons, respectively. The potential terms $\hat{V}_{nn}$, $\hat{V}_{ne}$, and $\hat{V}_{ee}$ are the interactions of nuclei-nuclei, nuclei-electron, and electron-electron, respectively.[2] While in theory this equation could be used to solve all quantum chemical problems, it is unfortunately impossible to solve for all but the simplest of systems (e.g., hydrogen atom). Fortunately, we can make several approximations to help simplify the complicated nature of this equation so as to enable at least accurate and reliable approximate solutions.

There are two approximations made to simplify the Hamiltonian and/or wavefunction. The first is the Born Oppenheimer approximation which effectively states that due to the fact that the nuclei are significantly heavier and slower than the electrons, that from the perspective of the electrons the nuclei can be considered stationary.[3] Consequently, the kinetic energy of the nuclei is zero, and the potential energy of nuclei-nuclei interactions is a constant and can be calculated separately and added back in when needed.

The second approximation that we commonly invoke is the Molecular Orbital approximation in which the motions of the electrons can be assumed to be independent of each other.[4] As a result, the wavefunction can be written as a product of 1-electron functions. This creates 1-electron orbitals that are much easier to solve. Furthermore, it facilitates replacement of the two-electron potential energy electron-electron term, with what is effectively a one-electron term.[5] Fortunately, there are methods that have been developed to incorporate electron correlation, but

they come at significant computational costs. Thankfully, other methods have been developed that can accurately describe large chemical systems at a relatively low computational cost, that is density functional theory (DFT).

Instead of gaining chemical insight through the wavefunction, density functional theory looks for a physically observable quality, the electron density.[5] Wavefunction methods are defined by four components; three spatial coordinates and one spin component. DFT removes the spin component and relies on the three spatial coordinates x, y, and z. It is for this reason DFT is less computationally taxing than wavefunction based methods. There are several different branches within DFT itself, however the common way to approach enzymatic systems has been through employing hybrid functionals. Hybrid functionals, like B3LYP, allows for a degree of electron exchange to be calculated.[6-8] Other approaches, such as the M06 suite, have been found to help describe non-bonded and long range interactions.[9,10] Overall, DFT has been extremely successful in describing biochemical models and has become a standard approach for analyzing enzymatic systems at the atomic level.[11,12]

2.3 Molecular Mechanics

A common theme in computational chemistry is the balance of accurately describing a chemical system while maintaining reasonable costs. In a perfect world, every chemical system would be described with the highest accuracy possible, unfortunately our resources are limited. This is an especially important consideration when analyzing large systems such as proteins, which contain thousands of atoms. The exceedingly clever computational chemists of the past have created a compromise between cost and accuracy. To appreciate the particular approach of molecular mechanics (MM) we must return to our understanding of conventional physics.

While our primary focus for quantum mechanic approaches are electrons, we ignore electrons in molecular mechanics and focus strictly on nuclei.[1] As one might expect, this eliminates the possibility of investigating any bond breaking/formation and therefore transition states. However, we now have a less computationally taxing way of representing bond distances, angles, dihedrals, van der Waals, and electrostatic interactions (Figure 2.1).

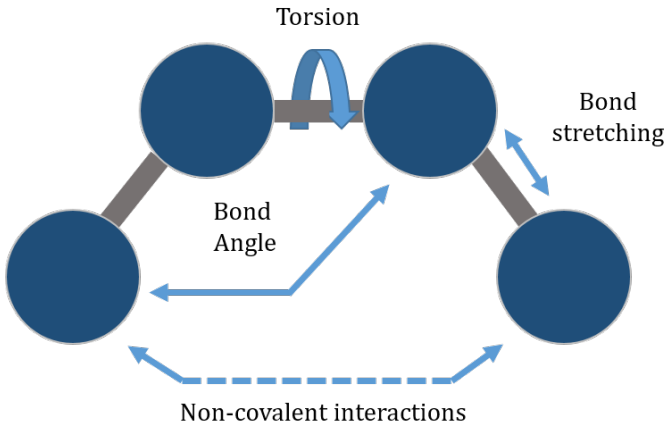

Figure 2.1 A ball and stick representation of the various forces calculated by molecular mechanics.

Molecular mechanics allows for a description of the energy through a combination of these covalent and non-covalent interactions (Equation 2.4).

$$E_{total} = E_{bond} + E_{angle} + E_{torsion} + E_{electrostatic} + E_{vdW} \qquad \textbf{Eq 2.4}$$

The E_{bond}, E_{angle}, and $E_{torsion}$ terms represent the bond stretching, angle bending and angle torsion, respectively. While the $E_{electrostatic}$ and E_{vdW} term make up the non-covalent electrostatics and van der Waal interactions, respectively.[1] It is important to note that molecular mechanics is an empirical approach and therefore

relies upon parameters obtained from accurate high level *ab initio* calculations or from experiment. Fortunately, a variety of different force fields exist to accurately describe different systems.[13-15] The force field used in this thesis is the Assisted Modeling Building with Energy Refinement (AMBER), an MM force field specifically designed for proteins and nucleic acids.[15-17]

2.4 Molecular Dynamic Simulations and Enzymes

It is absolutely essential for a computational chemist to start with an appropriate starting structure when analyzing enzymatic systems. Proteins exist in a variety of conformations and assuming their structure is widely inaccurate. Determining a representative protein structure can be challenging, but fortunately, a plethora of structures have been elucidated through X-ray and NMR data and are found on the Protein Data Bank website.[18] Even though x-ray structures can provide an excellent starting point, we know that proteins are not static and are often described as fluid-like.[19] We can overcome this limitation by using molecular dynamic simulations. Molecular dynamics provide us insights on how these atoms behave over time while maintaining a reasonable computational cost.[20]

Before beginning our molecular dynamic simulations, there are several criteria we must consider to pick an appropriate starting structure from an X-ray crystallographic image. This includes consideration of the resolution to be confident in the structural properties and the form of the enzyme, i.e., is it in a non-reactive form or reactive. Additionally, we must consider what types of modifications have been done to the protein to enable for crystallization. This includes residue mutations or the use of substrate analogs or inhibitors. Finally, we must consider the organism from which this structure was obtained. By considering these factors, we can make an informed decision on which structure is the most appropriate for

the proposed study. Once an appropriate structure has been chosen, we can then begin setting up and running our molecular dynamic simulations.

Molecular dynamic simulations follow a cyclic scheme for generating their trajectories.[21] Before the simulation can begin hydrogen atoms and protonation states are assigned and the system is parameterized based on the force field chosen. The system is then solvated and minimized. A brief equilibration period occurs allowing for annealing and finally the simulation begins. Trajectories are predicted based on Newtonian physics. The simulation continually predicts trajectories until the assigned time is reached.

The length of the simulation is strictly dependent on the behaviour that is being investigated, that is to say, there is not a set time limit.[19] Once the simulation is complete, the trajectories are then analyzed through a variety of tools. Typically a cluster analysis is performed to pick a representative structure for subsequent calculations. We can also investigate the structural variation through a root-mean squared deviation analysis by picking residues of interest, such as those nearby the active site, and substrates if necessary.[22] It is not surprising that much insight can be gained through molecular dynamic simulations alone, however in order to capture the reaction coordinates along a specific pathway we must employ quantum chemical methods.

2.5 Quantum Mechanical Clusters and Proton Affinities

While molecular mechanics and, by extension, molecular dynamics provide a reasonably accurate way to describe conformational dynamics, it fails to describe bond breakage or bond formation. One particular way to overcome this limitation is to use a methodology known as quantum mechanical clusters.[23] These are simple models that contain a small number of atoms, all of which are described using a quantum mechanics approach. In this thesis, the QM-cluster models constructed

were described using DFT, the specific methods used for each system are described in the upcoming chapters. They were used to calculate the proton affinities of several amino acid side chains particularly histidine's imidazole and glutamate's carboxyl group. This is calculated by finding the energy difference between the protonated form and its equivalent deprotonated form (Equation 2.5).[24]

$$E_{proton\ affinity} = E_{deprotonated} - E_{protonated} \qquad \textbf{Eq 2.5}$$

2.6 Quantum Mechanic/Molecular Mechanic Models

For a long time, QM-clusters were the method of choice to study enzymatic systems and are still used today to give insights into possible transition structures.[25] They provide a means of including specific residues involved in catalysis, however, there are additional contributing factors that allow for a reaction to be enzymatically feasible. There is a different approach that can be taken and has gained much traction over the decades since DFTs development. It is known as the quantum mechanics/molecular mechanics method, or QM/MM for short and, as the name implies, provides a blend of quantum mechanics and molecular mechanics (Figure 2.2) Its implementation has been successfully applied to many enzymatic systems and was recognized with the Nobel prize in 2013.[26]

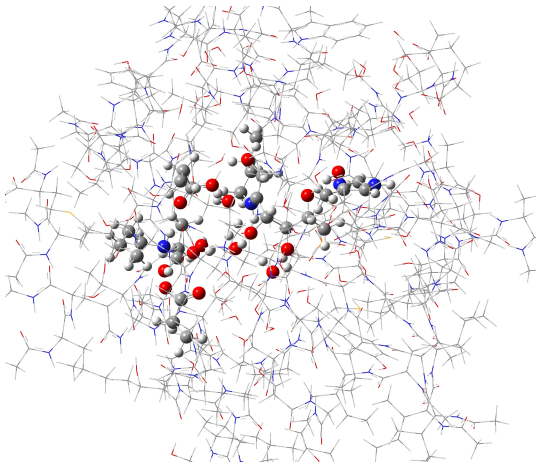

Figure 2.2 An example of a QM/MM model, the MM region is represented by the wireframe structure, the QM region is represented as ball and sticks.

A QM/MM model consists of two regions: a quantum mechanics region reserved for the significant residues, those involved in bond formation or breaking and/or stabilization of high energy transition states, and a molecular mechanics region which is made up of the remaining atoms.[27] It provides the higher accuracy afforded by QM calculations without having a large impact on the computational cost from the MM region.[28] This overcomes the limitation of QM-clusters by providing a way to represent the protein's environment rather than adding in corrections for it. Overall, there are two ways to represent a QM/MM model, subtractive and additive (Figure 2.3).[28,29]

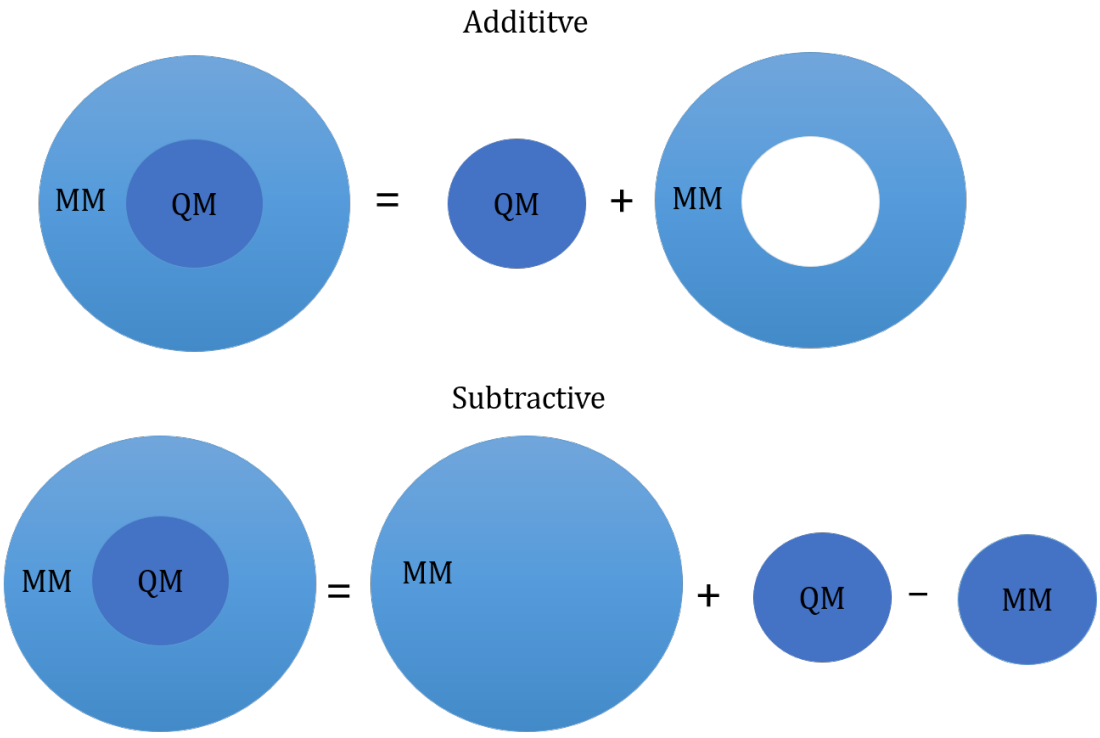

Figure 2.3 A representative illustration of the two coupling schemes for QM/MM models, additive and subtractive.

The additive method calculates the entirety of the MM region and QM region as follows in Equation 2.6:

$$E_{QM/MM} = E_{QM} + E_{MM} + E_{QM-MM} \qquad \textbf{Eq 2.6}$$

Where $E_{QM}$is the energy of the QM region, $E_{MM}$is the energy of the MM region and E_{QM-MM} is the interaction energy between the two regions.

Another approach, and the one specifically used in this thesis, is the subtractive method, also known as "Our own N-layered Integrated molecular Orbital molecular Mechanics" (ONIOM).[30] The ONIOM approach is as follows in Equation 2.7:

$$E_{ONIOM} = E_{MM} + E_{QM} - E_{MM\ (QM\ Region)} \quad \textbf{Eq 2.7}$$

Finally, it is important to consider how to appropriately set up a QM/MM model, specifically the boundary between the MM region and the QM region.[31] Generally, there are several guidelines to follow:

1. The boundary must be set at least 3 bonds away from any bond breaking/forming
2. The boundary must not be along a polar bond or cyclic structure.
3. The boundary should ideally be set between a non-polar C-C bond.
4. The boundary can only be represented by a single link atom.

Ideally, most of these guidelines should be followed when constructing a QM/MM model to ensure correct charge distribution throughout the QM layer. A common theme has been set throughout this chapter and also arises in the discussion of these guidelines; there is a balance between computational cost and accuracy. Although including a functional group some distance away from the bond formation/breaking is ideal, one must strongly consider the effective cost of that addition. Therefore, chemical intuition and understanding the limitations of a particular method of choice is extremely vital in constructing suitable representative models of enzymatic systems. Despite this, the ONIOM approach has been proven to be successful in accurately describing enzyme reactions.[32] It can successfully identify reaction pathways and transition states for a variety of enzymatic systems. It is clear computational enzymology is a powerful and exceptional tool for understanding these diverse natural catalysts.

2.7 Software

Several types of software suites were utilized throughout this thesis. In particular, molecular dynamic simulations were prepared and visualized using the Molecular Operating Environment (MOE)[33]. MDs were run using NAMD[34] and AMBER14[35]. VMD[36] was utilized for molecular dynamic visualization. All QM-cluster and QM/MM calculations were performed using the Gaussian 09 software package.[37] GaussView[38] was used to visualize all QM-cluster and QM/MM calculations.

2.8 References

(1) Cramer, C. J. Essentials of Computational Chemistry: Theories and Models; 2nd ed.; Wiley: Hoboken, NJ, 2004.

(2) Jensen, F. Introduction to Computational Chemistry; 2nd ed.; John Wiley & Sons: Hoboken, NJ, 2007.

(3) McQuarrie, D. A. Quantum Chemistry; University Science Books: Mill Valley, Calif., 1983.

(4) Young, D. C. Computational Chemistry: A Practical Guide for Applying Techniques to Real World Problems; Wiley: New York, 2001.

(5) Koch, W.; Holthausen, M. C. A Chemist's Guide to Density Functional Theory; 2nd ed.; Wiley-VCH: Weinheim ; New York, 2001.

(6) Becke, A. D. A New Mixing of Hartree-Fock and Local Density-Functional Theories. *J. Chem. Phys.* **1993**, *98*, 1372.

(7) Becke, A. D. Density-Functional Thermochemistry. 3. The Role of Exact Exchange. *J. Chem. Phys.* **1993**, *98*, 5648.

(8) Dickson, R. M.; Becke, A. D. Basis-Set-Free Local Density-Functional Calculations of Geometries of Polyatomic-Molecules. *J. Chem. Phys.* **1993**, *99*, 3898.

(9) Zhao, Y.; Truhlar, D. G. The M06 suite of density functionals for main group thermochemistry, thermochemical kinetics, noncovalent interactions, excited states, and transition elements: two new functionals and systematic testing of four M06-class functionals and 12 other functionals. *Theor. Chem. Acc.* **2008**, *120*, 215.

(10) Takatani, T.; Sears, J. S.; Sherrill, C. D. Assessing the Performance of Density Functional Theory For the Electronic Structure of Metal-Salens: The M06 Suite of Functionals and the d(4)-Metals. *J. Phys. Chem. A* **2010**, *114*, 11714.

(11) Gherib, R.; Dokainish, H. M.; Gauld, J. W. Multi-scale computational enzymology: enhancing our understanding of enzymatic catalysis. *Int. J. Mol. Sci.* **2014**, *15*, 401.

(12) Sousa, S. F.; Ribeiro, A. J. M.; Neves, R. P. P.; Brás, N. F.; Cerqueira, N. M. F. S. A.; Fernandes, P. A.; Ramos, M. J. Application of quantum mechanics/molecular mechanics methods in the study of enzymatic reaction mechanisms. *Wiley Interdiscip. Rev. Comput. Mol. Sci.* **2017**, *7*, e1281.

(13) Lee, J.; Cheng, X.; Swails, J. M.; Yeom, M. S.; Eastman, P. K.; Lemkul, J. A.; Wei, S.; Buckner, J.; Jeong, J. C.; Qi, Y.; Jo, S.; Pande, V. S.; Case, D. A.; Brooks, C. L., 3rd; MacKerell, A. D., Jr.; Klauda, J. B.; Im, W. CHARMM-GUI Input Generator for NAMD, GROMACS, AMBER, OpenMM, and CHARMM/OpenMM Simulations Using the CHARMM36 Additive Force Field. *J. Chem. Theory Comput.* **2016**, *12*, 405.

(14) Scott, W. R. P.; Hunenberger, P. H.; Tironi, I. G.; Mark, A. E.; Billeter, S. R.; Fennen, J.; Torda, A. E.; Huber, T.; Kruger, P.; van Gunsteren, W. F. The GROMOS biomolecular simulation program package. *J. Phys. Chem. A* **1999**, *103*, 3596.

(15) Wang, J.; Wolf, R. M.; Caldwell, J. W.; Kollman, P. A.; Case, D. A. Development and testing of a general amber force field. *J. Comput. Chem.* **2004**, *25*, 1157.

(16) Ponder, J. W.; Case, D. A. Force fields for protein simulations. *Adv. Protein Chem.* **2003**, *66*, 27.

(17) Cheatham, T. E.; Case, D. A. Twenty-Five Years of Nucleic Acid Simulations. *Biopolymers* **2013**, *99*, 969.

(18) Berman, H. M.; Westbrook, J.; Feng, Z.; Gilliland, G.; Bhat, T. N.; Weissig, H.; Shindyalov, I. N.; Bourne, P. E. The Protein Data Bank. *Nucleic Acids Res.* **2000**, *28*, 235.

(19) Henzler-Wildman, K.; Kern, D. Dynamic personalities of proteins. *Nature* **2007**, *450*, 964.

(20) Karplus, M.; Petsko, G. A. Molecular-Dynamics Simulations in Biology. *Nature* **1990**, *347*, 631.

(21) Dolinsky, T. J.; Czodrowski, P.; Li, H.; Nielsen, J. E.; Jensen, J. H.; Klebe, G.; Baker, N. A. PDB2PQR: expanding and upgrading automated preparation of biomolecular structures for molecular simulations. *Nucleic Acids Res.* **2007**, *35*, W522.

(22) Sargsyan, K.; Grauffel, C.; Lim, C. How Molecular Size Impacts RMSD Applications in Molecular Dynamics Simulations. *J. Chem. Theory Comput.* **2017**, *13*, 1518.

(23) Siegbahn, P. E. M.; Himo, F. The quantum chemical cluster approach for modeling enzyme reactions. *Wiley Interdiscip. Rev. Comput. Mol. Sci.* **2011**, *1*, 323.

(24) Bushnell, E. A. C.; Erdtman, E.; Llano, J.; Eriksson, L. A.; Gauld, J. W. The First Branching Point in Porphyrin Biosynthesis: A Systematic Docking, Molecular Dynamics and Quantum Mechanical/Molecular Mechanical Study of Substrate Binding and Mechanism of Uroporphyrinogen-III Decarboxylase. *J. Comput. Chem.* **2011**, *32*, 822.

(25) Sheng, X.; Himo, F. Theoretical Study of Enzyme Promiscuity: Mechanisms of Hydration and Carboxylation Activities of Phenolic Acid Decarboxylase. *ACS Catal.* **2017**, *7*, 1733.

(26) Thiel, W.; Hummer, G. Nobel 2013 Chemistry: Methods for computational chemistry. *Nature* **2013**, *504*, 96.

(27) Matta, C. F. Quantum Biochemistry; Wiley-VCH: Weinheim, 2010.

(28) Senn, H. M.; Thiel, W. QM/MM Methods for Biomolecular Systems. *Angew. Chem. Int. Edit.* **2009**, *48*, 1198.

(29) Rossbach, S.; Ochsenfeld, C. Influence of Coupling and Embedding Schemes on QM Size Convergence in QM/MM Approaches for the Example of a Proton Transfer in DNA. *J. Chem. Theory Comput.* **2017**, *13*, 1102.

(30) Morokuma, K.; Froese, R. D.; Dapprich, S.; Komaromi, I.; Khoroshun, D.; Byun, S.; Musaev, D. G.; Emerson, C. L. The ONIOM (our own integrated N-layered

molecular orbital and molecular mechanics) method, and its applications to calculations of large molecular systems. *Abstr. Pap. Am. Chem. Soc.* **1998**, *215*, U218.

(31) Clemente, F. R.; Vreven, T.; Frisch, M. J. Getting the Most out of ONIOM: Guidelines and Pitfalls In Quantum Biochemistry. Matta, C. (Ed.); Wiley-VCH: Weinheim, 2010; Vol. 2.

(32) Chung, L. W.; Sameera, W. M. C.; Ramozzi, R.; Page, A. J.; Hatanaka, M.; Petrova, G. P.; Harris, T. V.; Li, X.; Ke, Z. F.; Liu, F. Y.; Li, H. B.; Ding, L. N.; Morokuma, K. The ONIOM Method and Its Applications. *Chem. Rev.* **2015**, *115*, 5678.

(33) Molecular Operating Environment (MOE), 2013.08; Chemical Computing Group Inc: Montreal, Quebec, Canada, 2017.

(34) Phillips, J. C.; Braun, R.; Wang, W.; Gumbart, J.; Tajkhorshid, E.; Villa, E.; Chipot, C.; Skeel, R. D.; Kale, L.; Schulten, K. Scalable molecular dynamics with NAMD. *J. Chem. Theory Comput.* **2005**, *26*, 1781.

(35) Case, D. A.; Berryman, J. T.; Betz, R. M.; Cerutti, D. S.; Cheatham, III, T. E.; Darden, T. A.; Duke, R. E.; Giese, T. J.; Gohlke, H.; Goetz, A. W.; Homeyer, N.; Izadi, S.; Janowski, P.; Kaus, J.; Kovalenko, A.; Lee, T. S.; LeGrand, S.; Li, P.; Lin, C.; Luchko, T.; Luo, R.; Madej, B.; Merz, K. M.; Monard, G.; Needham, P.; Nguyen, H.; Nguyen, H. T.; Omelyan, I.; Onufriev, A.; Roe, D. R.; Roitberg, A.; Salomon-Ferrer, R.; Simmerling, C. L.; Smith, W.; Swails, J.; Walker, R. C.; Wang, J.; Wolf, R. M.; Wu, X.; York D. M.; Kollman, P. A. (2015), AMBER 2015, University of California, San Francisco.

(36) Humphrey, W.; Dalke, A.; Schulten, K. VMD: Visual molecular dynamics. *J. Mol. Graph. Model.* **1996**, *14*, 33.

(37) Frisch, M. J.; Trucks, G. W.; Schlegel, H. B.; Scuseria, G. E.; Robb, M. A.; Cheeseman, J. R.; Scalmani, G.; Barone, V.; Mennucci, B.; Petersson, G. A.; Nakatsuji, H.; Caricato, M.; Li, X.; Hratchian, H. P.; Izmaylov, A. F.; Bloino, J.; Zheng, G.; Sonnenberg, J. L.; Hada, M.; Ehara, M.; Toyota, K.; Fukuda, R.; Hasegawa, J.; Ishida, M.; Nakajima, T.; Honda, Y.; Kitao, O.; Nakai, H.; Vreven, T.; Montgomery, J., J. A. ; Peralta, J. E.; Ogliaro,

F.; Bearpark, M.; Heyd, J. J.; Brothers, E.; Kudin, K. N.; Staroverov, V. N.; Kobayashi, R.; Normand, J.; Raghavachari, K.; Rendell, A.; Burant, J. C.; Iyengar, S. S.; Tomasi, J.; Cossi, M.; Rega, N.; Millam, J. M.; Klene, M.; Knox, J. E.; Cross, J. B.; Bakken, V.; Adamo, C.; Jaramillo, J.; Gomperts, R.; Stratmann, R. E.; Yazyev, O.; Austin, A. J.; Cammi, R. P., C.; Ochterski, J. W.; Martin, R. L.; Morokuma, K.; Zakrzewski, V. G.; Voth, G. A.; Salvador, P.; Dannenberg, J. J.; Dapprich, S.; Daniels, A. D.; Farkas, Ö.; Foresman, J. B.; Ortiz, J. V.; Cioslowski, J. Fox, D. J. Gaussian 09, Gaussian, Inc., CT, Wallingford 2009.

(38) GaussView, Version 5, Dennington, R.; Keith, T.; Millam, J. Semichem Inc., Shawnee Mission, KS, 2009

Chapter 3:
The Inhibition Mechanism of CTX-M β-Lactamases

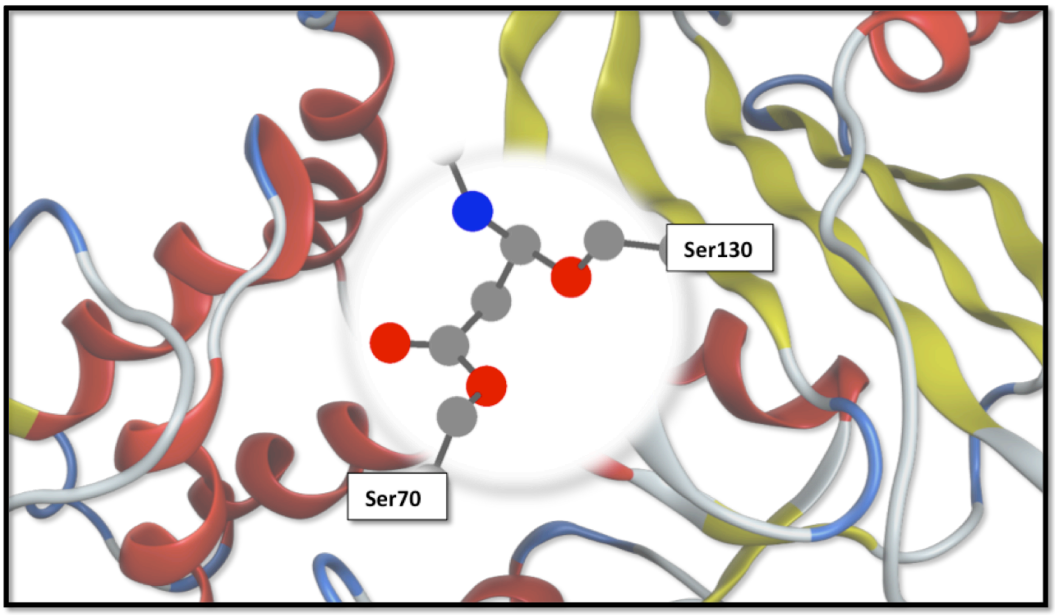

3.1 Introduction

The rise of antibiotic-resistant bacterial infections is a growing concern in the medical field and poses a serious threat to current treatments.[1,2] The widespread use of antibiotics has caused an emergence of bacterial populations capable of surviving the strongest antibiotics known to date.[3,4] One of the most common classes of antibiotics contain a β-lactam ring system; resistance to this class is brought about by the action of β-lactamase enzymes which hydrolytically cleave the β-lactam ring, rendering them ineffective.[5] This has raised concerns of their continued use in fear that one day they will become obsolete.[6]

β-lactamases are divided into four classes depending on their structure and function. Class B are a metallo-β-lactamase containing a zinc (II) ion in their active site, where as class A, C, D employ a serinyl-residue in their active site, believed to be responsible for hydrolyzing the lactam ring.[7,8] Overall their mechanism of action for the serinyl classes remains the same; hydrolysis of the lactam ring occurs in two steps (Scheme 3.1).[9-13] Once the substrate pencillin has bound to the active site (A), the serine nucleophilically attacks the carbonyl of the lactam in an acylation step to form an acyl-enzyme intermediate (B). This is followed by a deacylation reaction which hydrolyzes the covalent bond, releasing the inactivated drug and restoring the free enzyme (C).

Scheme 3.1. Reaction pathway of β-lactam antibiotic hydrolysis.

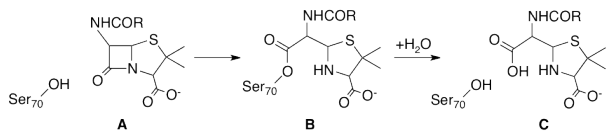

The CTX-M β-lactamase subclass is one of the most widespread extended-spectrum β-lactamases, named for their strong activity against cefotaxime (CTX)-

like antibiotics.[14] This subclass is commonly found in *E. coli*. Although they are considered a sub-class of the Class A β-lactamases, they have been shown to share less than 40% homology with the TEM and SHV Class A β-lactamases.[14] Their distinctive active site is smaller than their other Class A counterparts and it is believed the increased flexibility of their active site accounts for their increased activity against larger β-lactam antibiotics. Unfortunately the nuances of their active sites are poorly understood.[15]

To circumvent the action of β-lactamases, β-lactam antibiotics are often co-administered with lactamase inhibitors to prevent deactivation of the antibiotic.[16,17] The most commonly used inhibitors approved by the FDA are sulbactam, tazobactam, and clavulanic acid (Figure 3.1).[18] They employ a typical mechanism of inhibition, similar to the mechanism of antibiotic inactivation.[9-11] Specifically, Ser70 becomes deprotonated by Glu166 or Lys73 and then nucleophilically attacks the inhibitor's lactam ring.[19-21] Following the attack, an acylated intermediate is formed between the inhibitor and the Ser70 residue. While the formation of this covalent bond is commonly known, it has been discovered that there are alternatives to this pathway.[16]

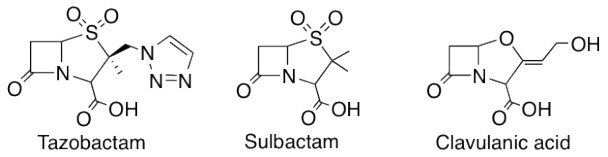

Figure 3.1. The chemical structure of the FDA approved β-lactamases inhibitors.

One strategy for developing inhibitors is to find a compound that has a greater affinity for the enzyme compared to antibiotics. Other factors are considered such as the rate of inhibition and IC50 concentrations.[22] This raises the question why the FDA inhibitors remain effective against CTX-M classes. The strategy for inhibition is

to prolong the deacylation step of the mechanism.[22] Therefore, if the inhibitors follow a similar pathway to antibiotic inactivation the deacylation step should be similar, however this is not the case. It was postulated that these inhibitors follow many different alternative pathways thus prolonging the deacylation step.[15]

A common mutation that occurs across Class A β-lactamases is the Ser130Gly mutant. Previous studies have shown that Ser130 appears to have two roles within the active site.[23] First, it participates in maintaining proper geometry for appropriate binding of inhibitors and lactam antibiotics. Secondly, the residue has been found to play a role in subsequent reactions that occur after Ser70's attack. In the case of the CTX-M Class A subclass, a recent study has identified a bridging intermediate formed in wild-type CTX-M β-lactamases, however it cannot be identified in the S130G mutant.[24]

While the covalent bond formation between Ser70 and the lactam ring is commonly known, Ser130 has been found to play a role during the pathway of inhibition. Following the formation of the covalent bond, Ser130 is capable of performing its own nucleophilic attack on the inhibitors. This forms a strong covalent cross-linked species between Ser70 and Ser130, thus stabilizing the acyl-enzyme intermediate and therefore providing a strong mode of inhibition (Scheme 3.2).[24] Although this has been identified as a known intermediate, it is unclear how it is formed. The deprotonation of Ser130 by a base can allow for its nucleophilic attack; however, the exact steps involved in the formation of the cross-linked intermediate are unknown.

It has been proposed that the formation of this cross-linked species is dependent on the conformation of the enzyme's active site.[24] The active site of CTX-M 9 has been shown to exist in two conformations. In conformation one a hydrogen bond is formed between Lys73 and Ser130, whereas in conformation two the hydrogen bond is not present. It is believed that the second conformation leads to

the formation of the cross-linked intermediate, allowing for the Ser130 to readily attack the amine. A few concerns arise from this assumption. Given the flexible nature of CTX-M's active site, one would expect that the formation would not solely depend on one hydrogen bond. While the presence of the hydrogen bond may affect the nucleophilic capabilities of Ser130 perhaps the flexible nature of the active site plays a more vital role. Investigating the nuances of this cross-linking reaction could lead to the design of stronger inhibitors.

Scheme 3.2. Reaction pathway of cross-linked species formation with tazobactam.[24]

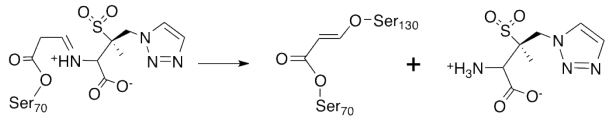

It is for this reason a variety of computational tools have been employed to investigate the complexity of this cross-linked species formation. Docking was performed on the non-active form of the enzyme to gain insight on the incorporation of the substrate. Molecular dynamics simulations were performed to provide insights on the specific inhibitor-enzyme interactions and the dynamics of its active site. QM/MM methods were used to provide insights on the reaction pathway. In this study, we have attempted to deliver atomistic insight on what drives the formation of the cross-linked species with the aim to provide opportunities for novel inhibitor design.

3.2 Computational Details

3.2.1 Molecular Docking

The X-ray structure of CTX-M-9 (PDB: 2P74) was used as the model for all subsequent simulations.[11] All water molecules and counter ions were removed and any non-native residues were reverted back to their native form. Tazobactam was manually docked into the active site using the X-ray structure CTX-M-9 linked to cefoxitin (PDB: 1YMX) as a template.[25]

3.2.2 Molecular Dynamics

Preparation and analysis of the molecular dynamic (MD) simulations were carried out within the Molecular Operating Environment (MOE) program suite.[26] All MD simulations were run with the NAMD program.[27] Protonation states of active site residues were assigned using PROPKA within MOE followed by layer solvation around the boundaries of the protein to 8 Å. Protonation states of active site residues were assigned using PROPKA in MOE.[28] The solvated, docked structure was minimized using the AMBER12:EHT molecular mechanics forcefield until the root mean square gradient of the total energy was below 0.21 kJ mol^{-1} $Å^{-1}$.[29,30]

The MD simulation was subjected to annealing at constant volume and pressure as the temperature was raised from 150 to 300 K over 150 ps. This was followed by a 20 ns production run until an active conformation was formed. All subsequent simulations were run using the active form as a starting structure. The reactive complex MD was subjected to a production run of 10ns while the intermediate complex of tazobactam covalently bound to Ser70 ran for 4 ns.

Cluster analysis was performed through root mean squared deviation of the active site residues and substrate. Through cluster analysis, the average structure with the most dominant conformation was obtained for each MD simulation and was used as a model for further QM/MM calculations.

3.2.3 QM/MM Calculations

All QM/MM calculations were performed using the ONIOM method in Gaussian 09 program suite.[31] Optimized structures were obtained using the ONIOM method, specifically ONIOM(M062X/6-31G(d):AMBER96) 5D.[32-34] Harmonic vibrational frequencies obtained at the optimization level of theory were conducted to identify the nature of the stationary points. Single point calculations were performed using ONIOM(M062X/6-311+G(2df,p) 5D:AMBER96) to obtain the relative energies.

All QM/MM models were truncated from the previously mentioned molecular dynamic simulations. All residues and water molecules 15 Å away from the substrate, tazobactam, were included. The QM-region contained the R-groups of Ser70, Lys73, Ser130, Asn132, Glu166, Ser273, Arg276 as well as the peptide backbone of Ser70 and Ser130. The surrounding residues were treated in the low layer with AMBER96 forcefield. All transition state structures were obtained through flexible scans with increments of 0.1 Å to 0.05 Å for refinement. This computational method of studying enzymes has been extensively used to characterize reactions, successfully identifying theoretical transition and intermediate structures and their relative energies.[35-37]

3.3 Results and Discussion

3.3.1 The Reactive Complex

The formation of the bridging intermediate is thought to be largely dependent on the conformation of Lys73 relative to Ser130, that is, the presence or absence of a hydrogen bond will dictate Ser130's involvement in the subsequent reaction. Herein, we explore various active site states through MD and QM/MM models. Specifically, we investigated the consequences of various protonation states: Lys73 as protonated or neutral. We also gained insights on the consequences of the S130G variant. Each MD model generated a QM/MM model to investigate the mechanistic

details. Figure 3.2 shows the MD results for the alternate protonation states. The RMSD produced by the MD simulation generated 10 clusters, each overlaid as shown in Figure 3.2A. This overlay shows Lys73 alternating a hydrogen bond between Ser130's oxygen and its carbonyl backbone. A distance plot measured between the $_{Lys73}N\cdots O_{Ser130}$ shows insignificant fluctuating between 2.6 to 3.6 Å (Figure 3.3A). The MD suggests that Lys73 may prefer to be in its protonated state.

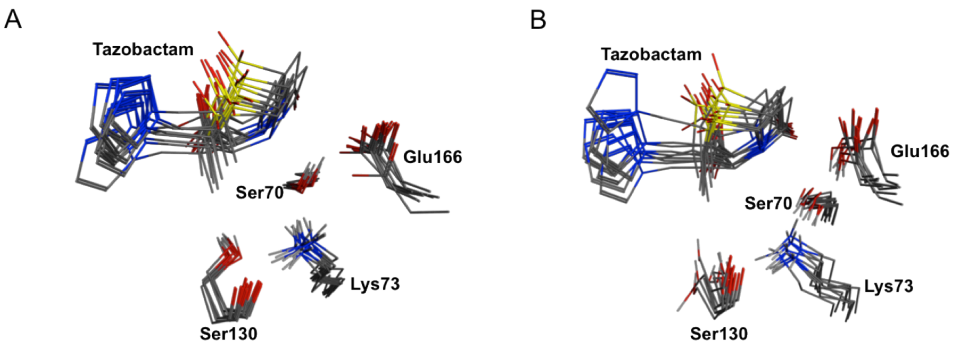

Figure 3.2. Overlays of structures obtained from cluster analysis of RMSD produced from 10ns production run of the reactive complex (A) Lys73 in its protonated state and (B) Lys73 in its neutral state.

As previously mentioned, the exact protonation states of Lys73 and Glu166 is a matter of debate. Although the PROPKA analysis of our model showed Lys73 in its protonated state, a separate MD was performed considering Lys73 and Glu166 as neutral. The RMSD of this particular run generated 10 clusters, an overlay is shown in Figure 3.2B. The protonation state of Lys73 seems to largely affect its interaction with Ser130's hydroxyl. A distance plot shows a greater variance compared to Lys73's protonated state, ranging from 2.6 to 5.6 Å (Figure 3.3B). The Lys73 residue maintains an interaction with Ser70's hydroxyl and Ser130's backbone carbonyl.

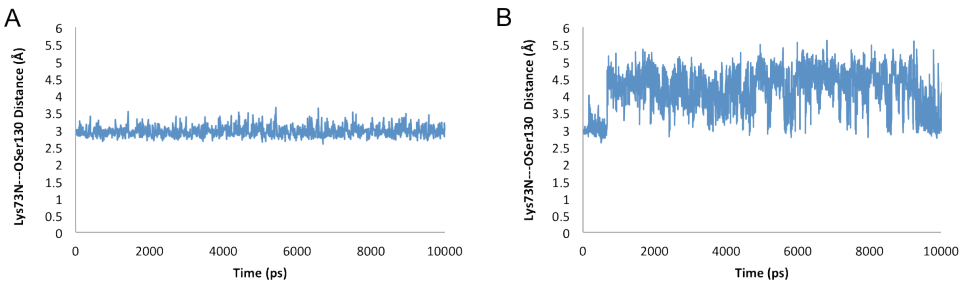

Figure 3.3. A distance plot of $_{Lys73}N\cdots O_{Ser130}$ over a 10ns production run of the reactive complex with (A) Lys73's protonated state and (B) Lys73's neutral state.

The impact of the S130G mutation was considered using an *in silico* mutagenesis MD run. The RMSD plot of this particular run shows high variance compared to the native active site, Figure 3.4A shows a cluster overlay produced from the RMSD. Surprisingly, the mutation largely impacted Ser70 causing it to exist in two conformations. Interestingly, Lys73 maintains a consistent hydrogen bond with Gly130's carbonyl backbone due to the lack of interaction with Ser130. The impact of this mutation could be from the large flexibility gained from the lack of Ser130's hydroxyl, which is apparent from its RMSD plot (Figure 3.4B). Specifically, the lack of interaction with Ser130's hydroxyl appears to affect the overall stability of the three other residues; Lys73, Ser70, and Glu166.

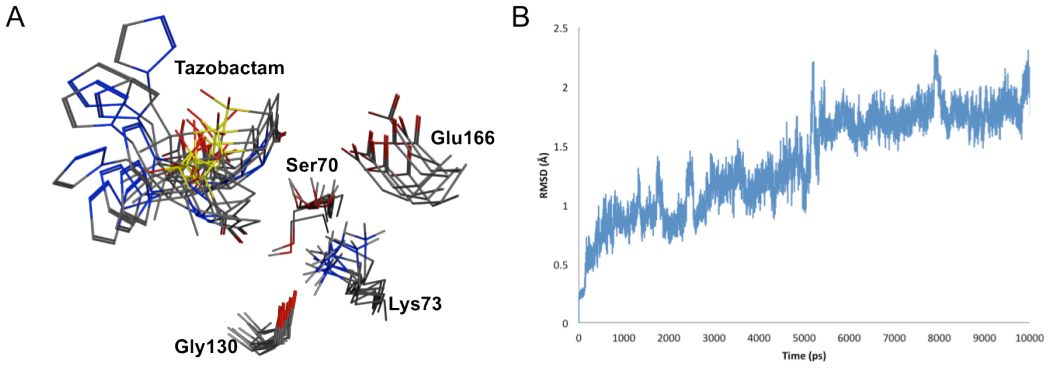

Figure 3.4. Overlay structures (A) obtained from cluster analysis of RMSD (B) produced from 10ns production run on the reactive complex of S130G variant.

We wished to explore the effects of the protonation state of Lys73 and the S130G variant on Ser70's β-hydroxyl distance towards the substrate (Figure 3.5). Although the protonation state appears to have an effect on Ser130's geometry, it appears to have little effect on Ser70's geometry. Interestingly, the S130G variant shows large variation in Ser70's motion with its distance ranging from 2.9 to 6.4 Å.

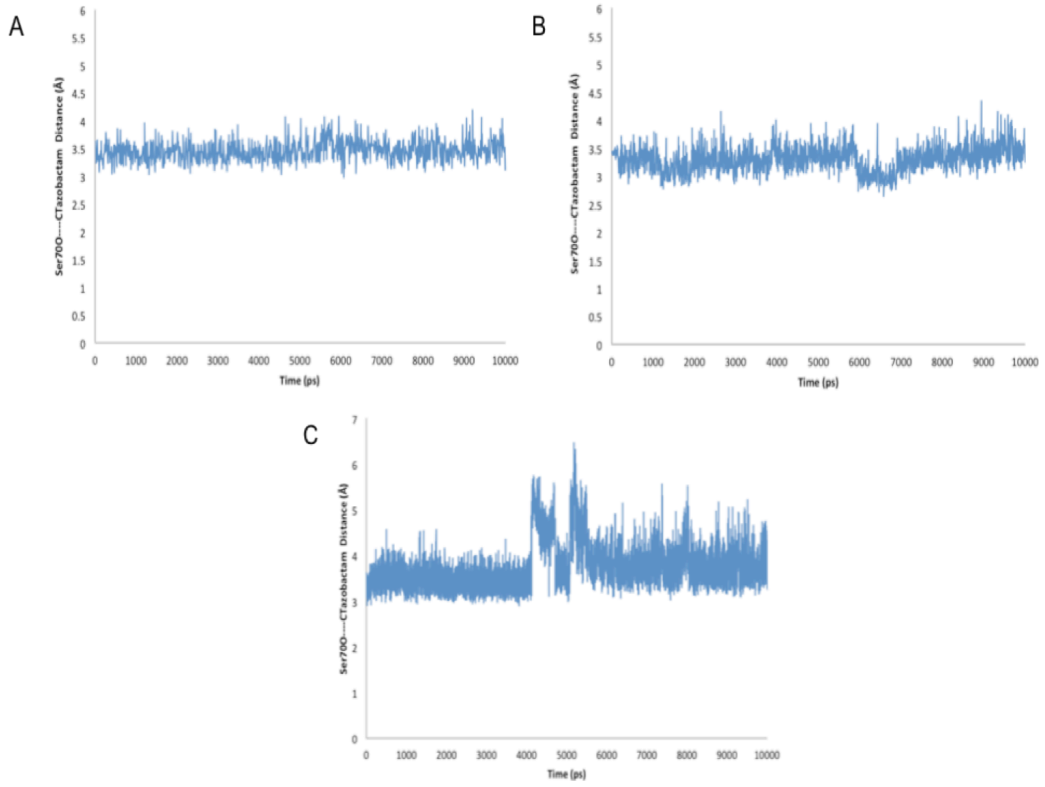

Figure 3.5. A distance plot produced from a 10ns production run on of the reaction complex of (A) Lys73 in its protonated state, (B) Lys73 in its neutral state, and (C) the S130G variant.

3.3.1.1 The Reactive Complex with Protonated Lys73

To gain further insight on the reactive complex, a QM/MM model was constructed from the highest average structure generated from the protonated

Lys73 MD run (Figure 3.6). We explored the nucleophilic attack of Ser70 on the substrate to determine the nature of Lys73 and Glu166 during the reaction. The optimized reactive complex (**RC$_{(Lys\text{-}H+)}$**) showed a distance of 2.83 Å between Ser70's β-hydroxyl and the carbonyl of tazobactam. The **RC$_{(Lys\text{-}H+)}$** shows Ser70's hydrogen of its β-hydroxyl pointing towards Glu166, suggesting it may act as a base during the reaction pathway. The transition state (**TS$_{(Lys\text{-}H+)}$**) does confirm Glu166's involvement as it abstracts Ser70's proton initiating the nucleophilic attack with an energetically favourable barrier of 66.0 kJ mol^{-1}.

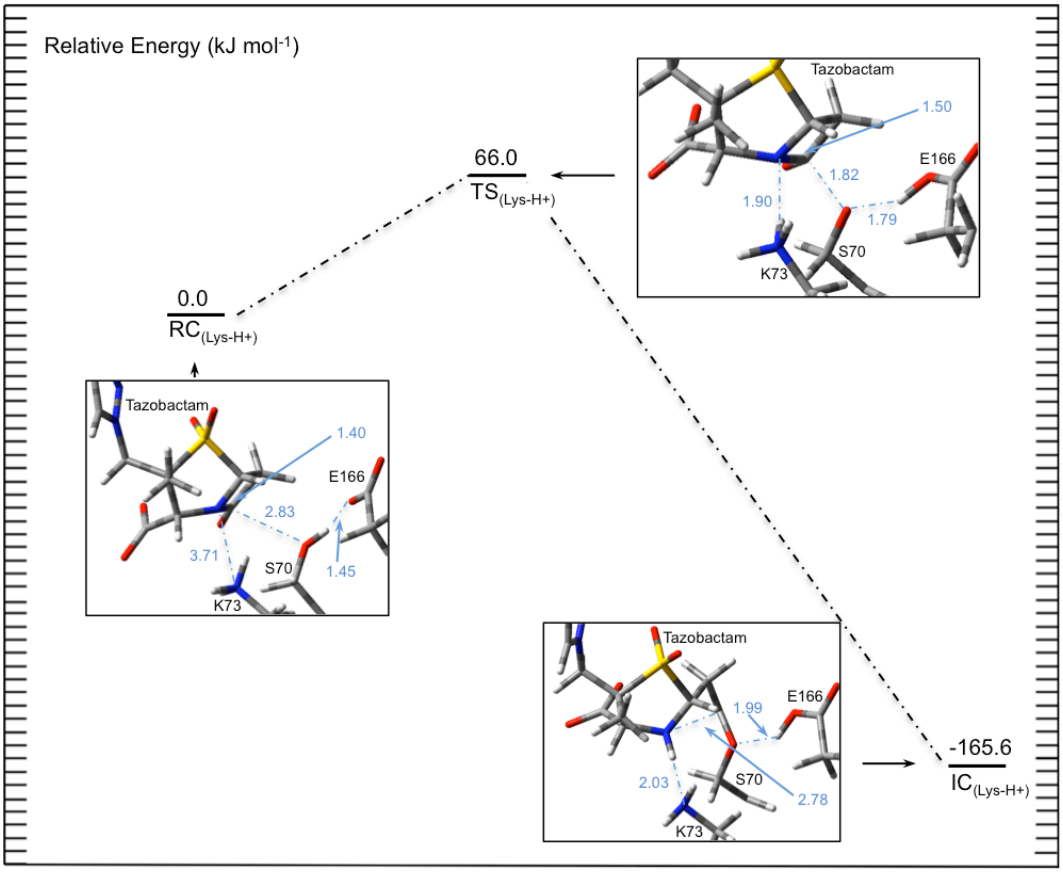

Figure 3.6. Relative energy surface obtained for the covalent formation of Ser70 to tazobactam, with Lys73 protonated and Glu166 deprotonated in **RC$_{(Lys\text{-}H+)}$**. See Computational Details.

The lactam ring amide bond increases from 1.40 Å to 1.50 Å during Ser70's approach. Moreover, **$TS_{(Lys\text{-}H+)}$** shows Lys73's involvement as it moves closer to the amine of the lactam ring placing it at 1.90 Å. By comparison, in the reactive complex it is 3.71 Å away. Finally, once the ring is open at a distance of 2.78 Å in the **$IC_{(Lys\text{-}H+)}$**, Lys73 donates its proton to the amine giving an energy value of −165.6 kJ mol^{-1}.

3.3.1.2 The Reactive Complex with Neutral Lys73

A model considering Lys73 as neutral was constructed to investigate whether the neutral form provided a reasonable pathway of inhibition (Figure 3.7). The **$RC_{(Lys\text{-}Neu)}$** shows Ser70 resting at distance of 3.14 Å away from the substrate, while a water molecule sits between Glu166 and Lys73. The water molecule also shares a hydrogen bond with the substrate at a distance of 1.95 Å.

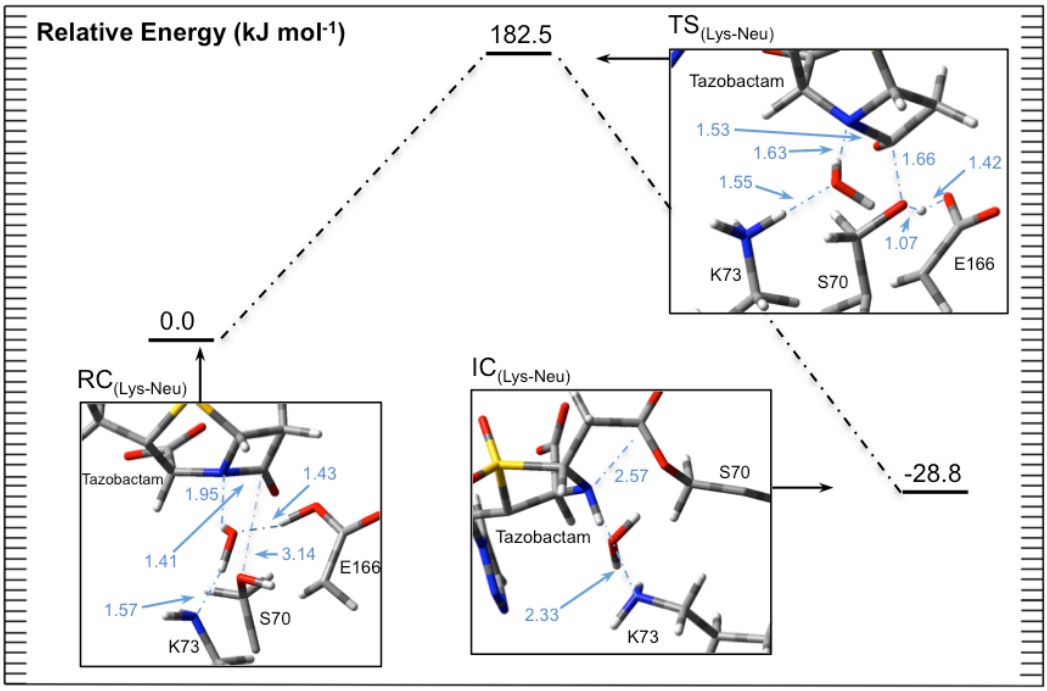

Figure 3.7. Relative energy surface obtained for the covalent formation of Ser70 to tazobactam, with Lys73 and Glu166 both neutral in **$RC_{(Lys\text{-}Neu)}$**. See Computational Details.

As Ser70's β-hydroxyl approaches the substrate, a concerted reaction occurs with a proton shuttled to the nearby Lys73 through the protonated Glu166 *via* a bridging water molecule. This leads to deprotonation of Ser70 from the newly deprotonated Glu166. This reaction proceeds through a late transition state, **$TS_{(Lys\text{-}Neu)}$**, which contains a protonated Lys73 residue that forms a hydrogen bond network towards the nitrogen in the lactam ring. Concomitantly, the ring opens slightly at a distance of 1.53 Å compared to 1.41 Å in its **$RC_{(Lys\text{-}Neu)}$**. Lys73 shuttles a proton through the water molecule producing a barrier of 182.5 kJ mol^{-1}. Ultimately this leads to the intermediate **$IC_{(Lys\text{-}Neu)}$** with Ser70 acylated at an energy of -28.8 kJ mol^{-1}. Interestingly, Lys73 that started the reaction in its neutral form finishes in the same state.

3.3.2 The Formation of the Bridging Intermediate

In contrast to the experimental observation, both **$IC_{(Lys\text{-}H+)}$** and **$IC_{(Lys\text{-}Neu)}$** was found to produce an unfavourable geometry for the attack of Ser130 on tazobactam. Thereby, we approached the model through another MD simulation. This simulation was performed on the intermediate complex of Ser70 covalently attached to tazobactam. This produced an RMSD with 9 clusters (Figure 3.8A). The MD run placed Ser130 in a favourable orientation for nucleophilic attack as Lys73 sits relatively close to act as a proton acceptor. This suggests Lys73 plays a possible role in its deprotonation allowing for the attack on the tazobactam intermediate. A distance plot measured between Ser130's oxygen and the expecting carbon that is supposed to attack shows a distance varying between 3.2 to 6.0 Å (Figure 3.8B).

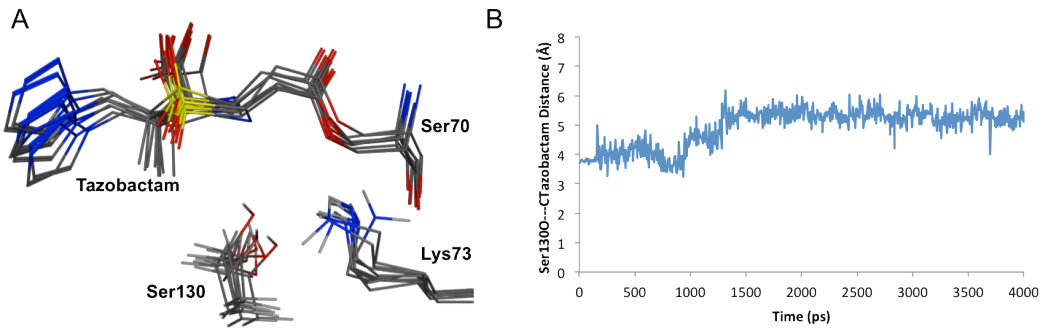

Figure 3.8. Overlay of structures (A) obtained from cluster analysis of RMSD produced from 4ns production run of the intermediate complex with Lys73 neutral. Distance plot (B) of Ser130's oxygen to tazobactam's carbon generated from 4ns production run with Lys73 neutral.

A model with the Lys73 protonated was considered, producing an RMSD with 10 clusters (Figure 3.9). Interestingly, Ser130 is placed in the proper orientation, however there is no base present to deprotonate Ser130. It would be unlikely for Ser130 to attack tazobactam without a readily available proton acceptor nearby.

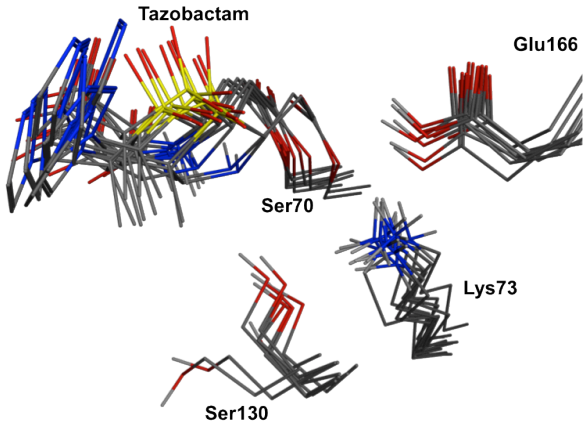

Figure 3.9. Overlay of structures obtained from cluster analysis of RMSD produced from 4ns production run of the intermediate complex with Lys73 protonated.

This highlights the importance of Lys73 acting as a proton donor during the formation of Ser70's covalent bond. Its neutral state during the intermediate complex places it in optimal proximity to Ser130 and leaves Ser130 in good orientation relative to tazobactam.

An MD run considering the mutant S130G was performed to explore the impact of this mutation on the intermediate complex. A RMSD analysis generated 9 clusters, overlaid in Figure 3.10A. Interestingly, this showed little variation compared to the reactive complex MD simulation in Figure 3.4. This may suggest that the mutation has a deeper impact on the initial reaction of Ser70's attack on the lactam ring, while not having much of an effect once the covalent bond is formed.

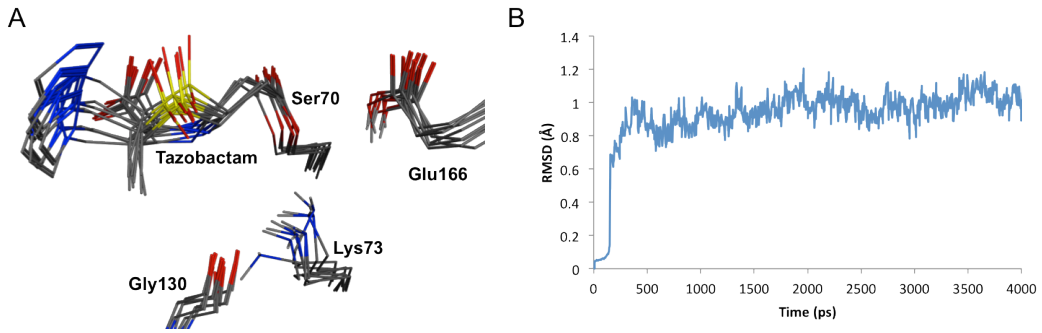

Figure 3.10. Overlay structures (A) obtained from cluster analysis of RMSD (B) produced from 4ns production run on the intermediate complex of S130G variant.

A QM/MM model was constructed from the most frequent cluster generated from the Lys73 neutral MD run. As stated previously, this model was considered for further insight as it provided Ser130 with reasonable orientation and, more importantly, provided a base for its β-hydroxyl's proton abstraction. The optimized **IC_1** places the attacking oxygen 2.57 Å away from the substrate while orientating its hydrogen 1.83 Å away from Lys73's nitrogen (Figure 3.11). Interestingly, the

sulfone has dissociated from its ring configuration, showing a distance of 3.14 Å. This places the nitrogen-carbon bond at 1.28 Å giving a double bond characteristic.

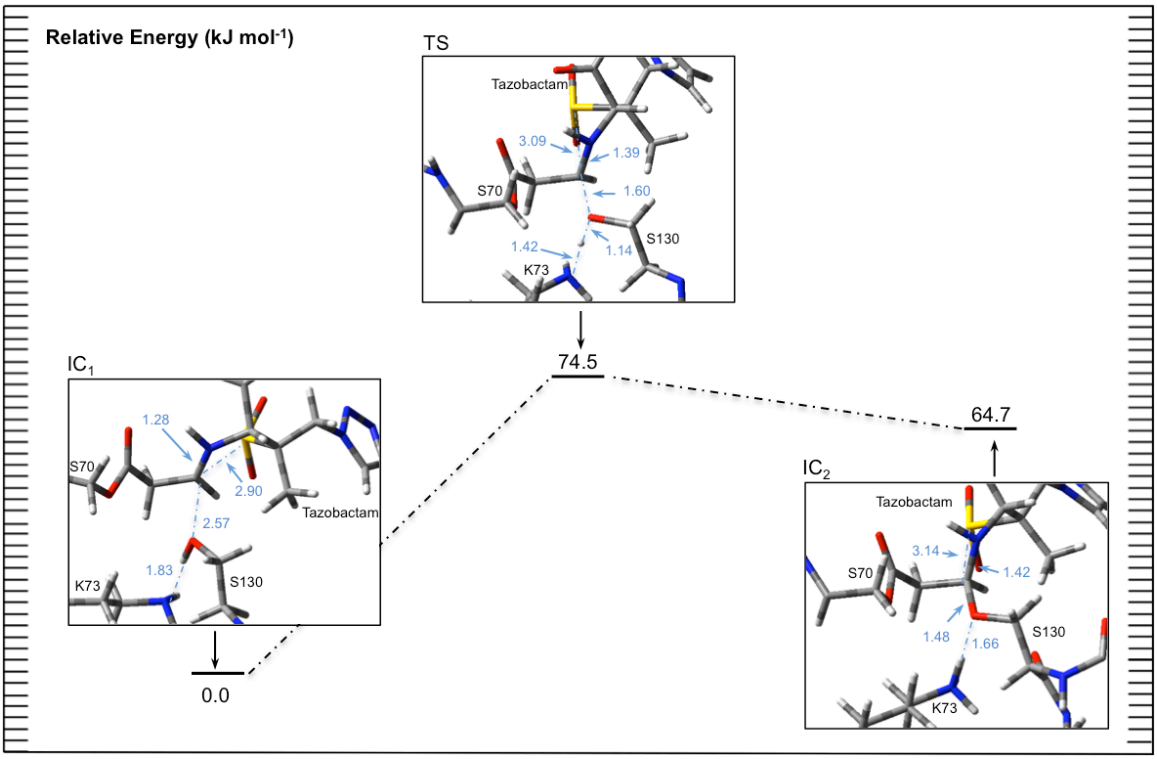

Figure 3.11. Relative energy surface obtained for the covalent formation of Ser130 to tazobactam intermediate, see Computational Details.

In **TS**, Ser130's nucleophilic oxygen is placed at a distance of 1.60 Å from the substrate while its proton is directed towards Lys73 at a distance of 1.14 Å. The nitrogen-carbon bond has extended to 1.39 Å. Indeed, the attack of Ser130 to tazobactam begins with its hydroxyl being deprotonated by Lys73 (**TS**), producing an energy barrier of 74.5 kJ mol^{-1}, relative to **IC$_1$**. Finally the bridging complex (**IC$_2$**) is formed with a relative energy of 64.7 kJ mol^{-1} forming a bond length of 1.48 Å. The sulfinate remains dissociated at a distance of 3.14 Å while the nitrogen-carbon bond retains a single bond at a distance of 1.42 Å.

3.4 Conclusion

We have explored the inhibition mechanism of CTX-M β-lactamases through a molecular dynamic approach while considering various reaction pathways through QM/MM methodology. Specifically, we explored the impact of Ser130's involvement during the reaction pathway. We've indicated Ser130's involvement in two ways while highlighting the importance of the protonation states of both Glu166 and Lys73.

Ser130 appears to have two roles in the active site of CTX-M β-lactamases. It provides stability to the reactive complex through a hydrogen bond interaction with Lys73 and provides a separate nucleophilic attack on the covalently bonded substrate after Ser70's attachment. While Lys73's conformation does change slightly, its conformation has a less impact on the bridge formation than previously proposed. More importantly, the orientation of the intermediate complex once Ser70 has covalently bonded to the substrate provides an opportunity for Lys73 to deprotonate Ser130.

Additionally, we've outlined the implications of Glu166 and Lys73 protonation states and perhaps further complicates the debate. Based on our models, Lys73 can be in its protonated state or its neutral state during Ser70's covalent bond formation. In the case of Lys73 being protonated, Glu166 acts as the base for Ser70 while Lys73 is able to readily donate its proton to the amine of the lactam ring. While in the alternative case, Lys73 acting as the base, we've found that Lys73 becomes protonated by Glu166 through a mediating water molecule and then Ser70 is deprotonated through Glu166's carboxylate. Both scenarios provide a reaction pathway in which Lys73 is later neutral, allowing for it to act as the base during Ser130's nucleophilic attack.

3.5 References

(1) Neu, H. C. The Crisis in Antibiotic-Resistance. *Science* **1992**, *257*, 1064.

(2) Laxminarayan, R.; Duse, A.; Wattal, C.; Zaidi, A. K. M.; Wertheim, H. F. L.; Sumpradit, N.; Vlieghe, E.; Hara, G. L.; Gould, I. M.; Goossens, H.; Greko, C.; So, A. D.; Bigdeli, M.; Tomson, G.; Woodhouse, W.; Ombaka, E.; Peralta, A. Q.; Qamar, F. N.; Mir, F.; Kariuki, S.; Bhutta, Z. A.; Coates, A.; Bergstrom, R.; Wright, G. D.; Brown, E. D.; Cars, O. Antibiotic resistance-the need for global solutions. *Lancet Infect. Dis.* **2013**, *13*, 1057.

(3) Rodriguez-Rojas, A.; Rodriguez-Beltran, J.; Couce, A.; Blazquez, J. Antibiotics and antibiotic resistance: A bitter fight against evolution. *Int. J. Med. Microbiol.* **2013**, *303*, 293.

(4) McGann, P.; Snesrud, E.; Maybank, R.; Corey, B.; Ong, A. C.; Clifford, R.; Hinkle, M.; Whitman, T.; Lesho, E.; Schaecher, K. E. Escherichia coli Harboring mcr-1 and bla(CTX-M) on a Novel IncF Plasmid: First Report of mcr-1 in the United States. *Antimicrob. Agents Ch.* **2016**, *60*, 4420.

(5) Fisher, J. F.; Meroueh, S. O.; Mobashery, S. Bacterial resistance to beta-lactam antibiotics: Compelling opportunism, compelling opportunity. *Chem. Rev.* **2005**, *105*, 395.

(6) Rossolini, G. M.; Arena, F.; Pecile, P.; Pollini, S. Update on the antibiotic resistance crisis. *Curr. Opin. Pharmacol.* **2014**, *18*, 56.

(7) Majiduddin, F. K.; Materon, I. C.; Palzkill, T. G. Molecular analysis of beta-lactamase structure and function. *Int. J. Med. Microbiol.* **2002**, *292*, 127.

(8) Bush, K. Metallo-beta-lactamases: A class apart. *Clin. Infect. Dis.* **1998**, *27*, S48.

(9) Farina, D.; Spyrakis, F.; Venturelli, A.; Cross, S.; Tondi, D.; Costi, M. P. The Inhibition of Extended Spectrum beta-Lactamases: Hits and Leads. *Curr. Med. Chem.* **2014**, *21*, 1405.

(10) Meroueh, S. O.; Fisher, J. F.; Schlegel, H. B.; Mobashery, S. Ab initio QM/MM study of class A beta-lactamase acylation: Dual participation of Glu166 and Lys73 in a concerted base promotion of Ser70. *J. Am. Chem. Soc.* **2005**, *127*, 15397.

(11) Chen, Y.; Bonnet, R.; Shoichet, B. K. The acylation mechanism of CTX-M beta-lactamase at 0.88 angstrom resolution. *J. Am. Chem. Soc.* **2007**, *129*, 5378.

(12) Minasov, G.; Wang, X. J.; Shoichet, B. K. An ultrahigh resolution structure of TEM-1 beta-lactamase suggests a role for Glu166 as the general base in acylation. *J. Am. Chem. Soc.* **2002**, *124*, 5333.

(13) Hermann, J. C.; Hensen, C.; Ridder, L.; Mulholland, A. J.; Holtje, H. D. Mechanisms of antibiotic resistance: QM/MM modeling of the acylation reaction of a class A beta-lactamase with benzylpenicillin. *J. Am. Chem. Soc.* **2005**, *127*, 4454.

(14) Chen, Y.; Delmas, J.; Sirot, J.; Shoichet, B.; Bonnet, R. Atomic resolution structures of CTX-M beta-lactamases: Extended spectrum activities from increased mobility and decreased stability. *J. Mol. Biol.* **2005**, *348*, 349.

(15) Bethel, C. R.; Taracila, M.; Shyr, T.; Thomson, J. M.; Distler, A. M.; Hujer, K. M.; Hujer, A. M.; Endimiani, A.; Papp-Wallace, K.; Bonnet, R.; Bonomo, R. A. Exploring the Inhibition of CTX-M-9 by beta-Lactamase Inhibitors and Carbapenems. *Antimicrob. Agents Ch.* **2011**, *55*, 3465.

(16) Drawz, S. M.; Bonomo, R. A. Three Decades of beta-Lactamase Inhibitors. *Clin. Microbiol. Rev.* **2010**, *23*, 160.

(17) Walsh, C. Molecular mechanisms that confer antibacterial drug resistance. *Nature* **2000**, *406*, 775.

(18) Biondi, S.; Long, S.; Panunzio, M.; Qin, W. L. Current Trends in beta-Lactam Based beta-Lactamases Inhibitors. *Curr. Med. Chem.* **2011**, *18*, 4223.

(19) Hermann, J. C.; Pradon, J.; Harvey, J. N.; Mulholland, A. J. High Level QM/MM Modeling of the Formation of the Tetrahedral Intermediate in the Acylation

of Wild Type and K73A Mutant TEM-1 Class A beta-Lactamase. *J. Phys. Chem. A* **2009**, *113*, 11984.

(20) Vandavasi, V. G.; Weiss, K. L.; Cooper, J. B.; Erskine, P. T.; Tomanicek, S. J.; Ostermann, A.; Schrader, T. E.; Ginell, S. L.; Coates, L. Exploring the Mechanism of beta-Lactam Ring Protonation in the Class A beta-lactamase Acylation Mechanism Using Neutron and X-ray Crystallography. *J. Med. Chem.* **2016**, *59*, 474.

(21) Hermann, J. C.; Ridder, L.; Mulholland, A. J.; Holtje, H. D. Identification of Glu166 as the general base in the acylation reaction of class A beta-lactamases through QM/MM modeling. *J. Am. Chem. Soc.* **2003**, *125*, 9590.

(22) Sulton, D.; Pagan-Rodriguez, D.; Zhou, X.; Liu, Y. D.; Hujer, A. M.; Bethel, C. R.; Helfand, M. S.; Thomson, J. M.; Anderson, V. E.; Buynak, J. D.; Ng, L. M.; Bonomo, R. A. Clavulanic acid inactivation of SHV-1 and the inhibitor-resistant S130G SHV-1 beta-lactamase - Insights into the mechanism of inhibition. *J. Biol. Chem.* **2005**, *280*, 35528.

(23) D'andrea, M. M.; Arena, F.; Pallecchi, L.; Rossolini, G. M. CTX-M-type beta-lactamases: A successful story of antibiotic resistance. *Int. J. Med. Microbiol.* **2013**, *303*, 305.

(24) Heidari-Torkabadi, H.; Bethel, C. R.; Ding, Z.; Pusztai-Carey, M.; Bonnet, R.; Bonomo, R. A.; Carey, P. R. "Mind the Gap": Raman Evidence for Rapid Inactivation of CTX-M-9 beta-Lactamase Using Mechanism-Based Inhibitors that Bridge the Active Site. *J. Am. Chem. Soc.* **2015**, *137*, 12760.

(25) Chen, Y.; Shoichet, B.; Bonnet, R. Structure, function, and inhibition along the reaction coordinate of CTX-M beta-lactamases. *J. Am. Chem. Soc.* **2005**, *127*, 5423.

(26) Molecular Operating Environment (MOE), 2013.08; Chemical Computing Group Inc: Montreal, Quebec, Canada, 2017.

(27) Phillips, J. C.; Braun, R.; Wang, W.; Gumbart, J.; Tajkhorshid, E.; Villa, E.; Chipot, C.; Skeel, R. D.; Kale, L.; Schulten, K. Scalable molecular dynamics with NAMD. *J. Chem. Theory Comput.* **2005**, *26*, 1781.

(28) Rostkowski, M.; Olsson, M. H. M.; Sondergaard, C. R.; Jensen, J. H. Graphical analysis of pH-dependent properties of proteins predicted using PROPKA. *BMC Struct. Biol.* **2011**, *11*.

(29) Cornell, W. D.; Cieplak, P.; Bayly, C. I.; Gould, I. R.; Merz, K. M.; Ferguson, D. M.; Spellmeyer, D. C.; Fox, T.; Caldwell, J. W.; Kollman, P. A. A second generation force field for the simulation of proteins, nucleic acids, and organic molecules (vol 117, pg 5179, 1995). *J. Am. Chem. Soc.* **1996**, *118*, 2309.

(30) Salomon-Ferrer, R.; Case, D. A.; Walker, R. C. An overview of the Amber biomolecular simulation package. *Wiley Interdiscip. Rev. Comput. Mol. Sci.* **2013**, *3*, 198.

(31) Frisch, M. J.; Trucks, G. W.; Schlegel, H. B.; Scuseria, G. E.; Robb, M. A.; Cheeseman, J. R.; Scalmani, G.; Barone, V.; Mennucci, B.; Petersson, G. A.; Nakatsuji, H.; Caricato, M.; Li, X.; Hratchian, H. P.; Izmaylov, A. F.; Bloino, J.; Zheng, G.; Sonnenberg, J. L.; Hada, M.; Ehara, M.; Toyota, K.; Fukuda, R.; Hasegawa, J.; Ishida, M.; Nakajima, T.; Honda, Y.; Kitao, O.; Nakai, H.; Vreven, T.; Montgomery, J., J. A. ; Peralta, J. E.; Ogliaro, F.; Bearpark, M.; Heyd, J. J.; Brothers, E.; Kudin, K. N.; Staroverov, V. N.; Kobayashi, R.; Normand, J.; Raghavachari, K.; Rendell, A.; Burant, J. C.; Iyengar, S. S.; Tomasi, J.; Cossi, M.; Rega, N.; Millam, J. M.; Klene, M.; Knox, J. E.; Cross, J. B.; Bakken, V.; Adamo, C.; Jaramillo, J.; Gomperts, R.; Stratmann, R. E.; Yazyev, O.; Austin, A. J.; Cammi, R. P., C.; Ochterski, J. W.; Martin, R. L.; Morokuma, K.; Zakrzewski, V. G.; Voth, G. A.; Salvador, P.; Dannenberg, J. J.; Dapprich, S.; Daniels, A. D.; Farkas, Ö.; Foresman, J. B.; Ortiz, J. V.; Cioslowski, J. Fox, D. J. Gaussian 09, Gaussian, Inc., CT, Wallingford 2009

(32) Vreven, T.; Byun, K. S.; Komaromi, I.; Dapprich, S.; Montgomery, J. A.; Morokuma, K.; Frisch, M. J. Combining quantum mechanics methods with molecular mechanics methods in ONIOM. *J. Chem. Theory Comput.* **2006**, *2*, 815.

(33) Chung, L. W.; Sameera, W. M. C.; Ramozzi, R.; Page, A. J.; Hatanaka, M.; Petrova, G. P.; Harris, T. V.; Li, X.; Ke, Z. F.; Liu, F. Y.; Li, H. B.; Ding, L. N.; Morokuma, K. The ONIOM Method and Its Applications. *Chem. Rev.* **2015**, *115*, 5678.

(34) Zhao, Y.; Truhlar, D. G. The M06 suite of density functionals for main group thermochemistry, thermochemical kinetics, noncovalent interactions, excited states, and transition elements: two new functionals and systematic testing of four M06-class functionals and 12 other functionals. *Theor. Chem. Acc.* **2008**, *120*, 215.

(35) Senn, H. M.; Thiel, W. QM/MM Studies of Enzymes. *Curr. Opin. Chem. Biol.* **2007**, *11*, 182.

(36) Dokainish, H. M.; Gauld, J. W. Formation of a Stable Iminol Intermediate in the Redox Regulation Mechanism of Protein Tyrosine Phosphatase 1B (PTP1B). *ACS Catal.* **2015**, *5*, 2195.

(37) Pinto, G. P.; Bras, N. F.; Perez, M. A. S.; Fernandes, P. A.; Russo, N.; Ramos, M. J.; Toscano, M. Establishing the Catalytic Mechanism of Human Pancreatic alpha-Amylase with QM/MM Methods. *J. Chem. Theory Comput.* **2015**, *11*, 2508.

Chapter 4:
Ring Opening Mechanism of Glucosamine-6-Phosphate Synthase

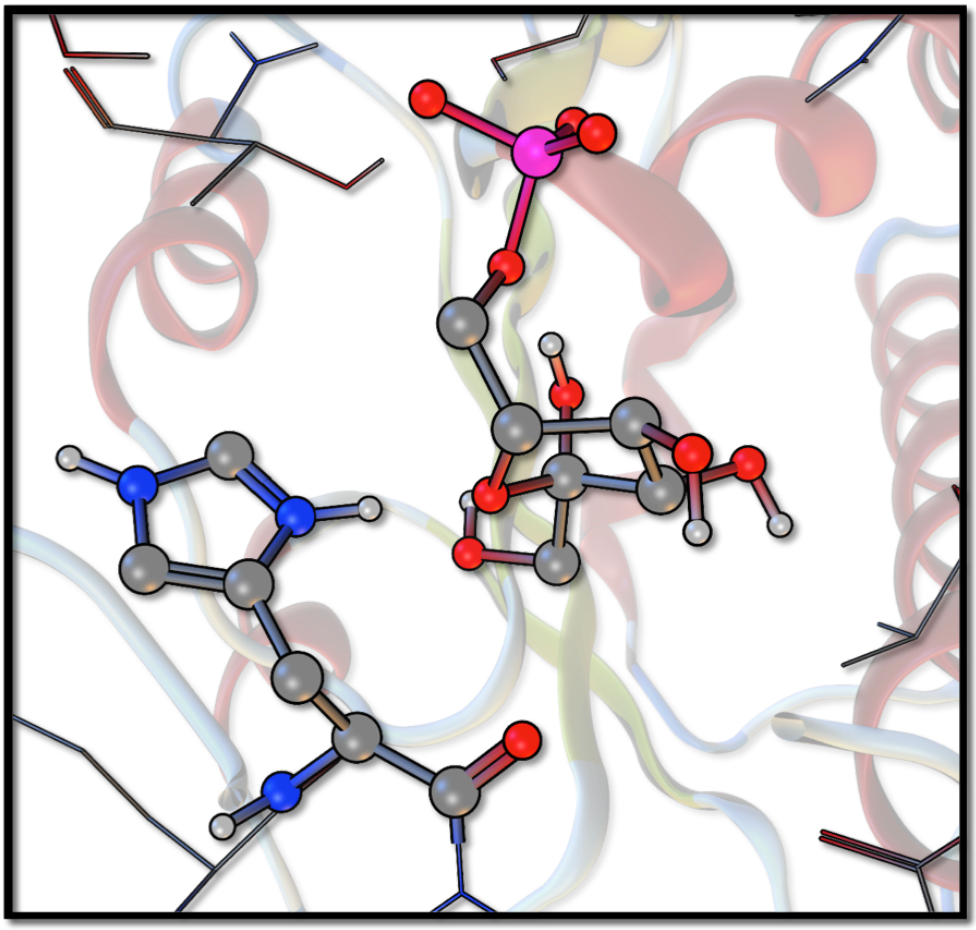

4.1 Introduction

Glucosamine-6-phosphate synthase (GlmS) is a critical enzyme in the biosynthesis of hexosamines. It catalyzes the rate-limiting step of hexosamine formation *via* the conversion of fructose-6-phosphate to glucosamine-6-phosphate.[1] Ultimately, glucosamine-6-phosphate synthesis leads to the formation of UDP-N-acetylglucosamine. This product is a key molecule in the formation of bacteria's peptidoglycan and fungi's chitin.[2,3] This has led to the investigation of GlmS as an antimicrobial target.[4,5] Moreover, human GlmS has been found to have a role in glucose regulation and implications towards diabetes.[6] Intriguingly, overexpression of glutamine:fructose-6-phosphate amidotransferase (GFA) genes in pancreatic cells of transgenic mice has led to insulin resistance and mild type II diabetes.[7] In addition, increased activity of GlmS, due to high glucose or glutamine concentration, leads to vascular dysfunction.[8] It is clear this enzyme has many physiological implications thus understanding its precise catalytic nature could potentially lead to the design of inhibitors.

GlmS belongs to a family of enzyme's known as amidotransferases, a class of enzymes responsible for the catalytic activity of glutamine's deamination to form glutamate and an aminated product.[9] Several members of this family are directly responsible for biosynthesis of purines and pyrimidines, amino acids, and other aminated products.[9-11] While most amidotransferases can use exogenous ammonia as a source of nitrogen, GlmS remains unique in that it requires glutamine as its strict source.[12] GlmS, therefore, contains two catalytic sites, one for the deamination of glutamine, the other responsible for the synthesis of glucosamine-6-phosphate from fructose-6-phosphate (Fru-6-P).[13]

GlmS is primarily responsible for the generation of glucosamine-6-phosphate, however each site can act individually.[14,15] Specifically, the enzyme catalyzes the hydrolysis of glutamine without the presence of Fru-6-P or, conversely,

isomerization of Fru-6-P occurs in the absence of glutamine. This highlights the complexity of the overall synthesis of glucosamine-6-phosphate. The reaction occurs in three steps, the generation of ammonia from glutamine hydrolysis, the transfer of the ammonia to Fru-6-P, and finally the generation of glucosamine-6-phosphate.[16] GlmS achieves this remarkable cooperativity through an 18 Å channel connecting both the deamination site and the synthase site.[17]

To prevent loss of ammonia to the outside environment, GlmS employs a protective mechanism *via* conformational changes.[18] Fru-6-P binds to the synthase site and undergoes ring opening, which begins to align the channel. Glutamine then binds to the glutaminase site and, prior to its hydrolysis, the channel opens and a protective Q-loop closes over the site.[18] The reaction produces glutamic acid and glucosamine-6-phosphate all while insuring the ammonia produced is not lost to the surrounding environment. The sequential binding of the substrates tightly regulates this process, which is initiated by the binding and ring opening of Fru-6-P.

Fru-6-P binds to the active site primarily through its phosphate group, forming a network of hydrogen bonds with Ser347, Gln348, Ser349, and Thr352. This places the substrate into the synthase site where Glu488, His504, and Lys603 have been found to be involved in the ring opening of Fru-6P and glucosamine-6-phosphate formation.[17] It has been proposed that the ring opening mechanism is strictly a result of the catalytic activity of His504.[19,20] Specifically, His504's imidazole ring is expected to sit in its neutral form, and this initiates deprotonation of Fru-6-P's O2 hydroxyl (Scheme 4.1). The ring begins to open and the newly formed oxyanion from the ether oxygen accepts a proton from H504. Indeed, kinetic analysis of a H504Q variant has shown decreased activity, suggesting its catalytic function.[18] A similar enzyme, glucosamine-6-phosphate deaminase, catalyzes the reverse reaction of glucosamine-6-phosphate to fructose-6-phoshate and ammonia. Interestingly, this enzyme has also been found to have a histidine involved its catalytic site acting

as both a proton acceptor and donor.[21,22] Other ring opening enzymes such as phosphoglucose isomerase employ an acid-base reaction with a catalytic triad of lysine, histidine and glutamic acid.[23]

The precise details of how GlmS catalyzes the ring opening of Fru-6-P remains debated. While the presence of H504 has been found to be catalytically important, other catalytic residues have been identified. Both Glu488 and Lys485 sit near the substrate, and are expected to act as proton acceptors in the subsequent reactions, suggesting they play a catalytic role in the active site.[18]

Scheme 4.1. Proposed reaction for fructose-6-phosphate ring opening catalyzed by GlmS.[18]

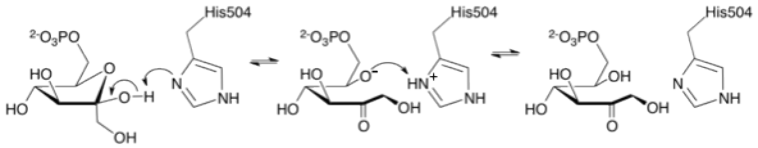

We have employed a multiscale computational approach to obtain detailed information about catalytic nature of GlmS's ring opening mechanism. Specifically, we used molecular dynamics and QM-cluster approaches to appreciate the potential interactions and protonation states of key residues. We've gained further atomistic insight through an ONIOM QM/MM approach providing details on the reaction pathway of the ring opening mechanism.

4.2 Computational Details

4.2.1 Sample Preparation

The X-ray structure of glucosamine-6-phosphate synthase from *Escherichia coli* (PDB: 2J6H) with glucose-6-phosphate and 5-oxo-L-norleucine was used as a

starting structure for all subsequent simulations.[13] 5-oxo-L-norleucine and glucose-6-phoshate were converted to glutamine and fructose-6-phosphate, respectively.

Protonation states were assigned with PROPKA[24,25], histidyls were protonated based on their environment excluding the protonation state of H504 where both states were considered. Topology and coordinate files were generated with tleap module of AMBER14.[26] Solvation was performed using 87921 TIP3P[27] water molecules in a cubic box with an edge length of ~141.1 Å**,** this achieved a density of 1.05g/cm after equilibration.

4.2.2 Molecular Dynamics

All MD simulations were performed using the AMBER14[26] program with graphics processing units version of pmemd.[28,29] The forcefields ff14SB[30] and TIP3P[27] were used to describe proteins and water molecules, respectively. Antechamber[31,32] was used to construct both glutamine and fructose-6-phosphate, using the ff14SB forcefield and RESP atomic charges. Gas phase optimizations at the HF/6-31G(d) level of theory within the Gaussian09[33] program were used to calculate the charges of glutamine and fructose-6-phosphate, each capped methyl groups. A cut-off of 8 Å was utilized in real space for long-range electrostatics using the Particle-Mesh Ewald (PME) procedure with periodic boundary conditions and NVT ensemble applied.[34] The SHAKE algorithm and a 2 fs timestep were used for equilibration and production by restricting the bond stretches from hydrogen atoms. Equilibration occurred in five stages following energy minimization; (1) a harmonic potential of 50 kcal mol^{-1} $Å^{-2}$ for 100 ps at 10 K was used to restrain proper geometry of hydrogen atoms and all heavy atoms; (2) to optimize positions of water with respect to the protein, the same potential and conditions were used for 100 ps but without restraint applied to the oxygens of water; (3) the protein heavy atoms harmonic potential restraint was decreased to 5 kcal mol^{-1} $Å^{-2}$ for 100 ps; (4) for 100.0 ps, the

harmonic potential was removed; and (5) over a period of 2000 ps the system was incrementally heated to 300 K. In stage 5 the velocities were updated every 100 steps, and every 10 steps for equilibration stages 1 to 4. Following equilibration, a production run of 100 ns was used.

4.2.3 QM/MM Calculations

The ONIOM method in Gaussian 09[33] suite program was used for all QM/MM calculations. ONIOM(B3LYP/6-31G(d):AMBER96) 5D was used to optimize all subsequent structures.[35-37] To access the nature of the stationary points, all optimized structures were analyzed through their harmonic vibrational frequencies obtained at the same level of theory as the optimized structures. Single point calculations were applied to the optimized structures using ONIOM(B3LYP/6-311+G(2df,p):AMBER96).

All QM/MM structures were obtained from the previously mentioned MD simulations. A representative structure was obtained through RMSD analysis choosing an appropriate structure once equilibration of the RMSD curve had been achieved. To represent the protein environment, all water molecules and residues 15 Å away from the substrate, Fru-6-P, were included. This produced a model of 1912 atoms. The substrate, Fru-6-P, and the R-groups of Glu396, Glu481, Lys485, Glu488, His504, Lys603, as well as several nearby waters were included in the QM-region, giving a total of 105 atoms. The AMBER96 forcefield was used for all other residues and waters in the low layer. Flexible scans with increments of 0.1 Å to 0.05 Å were used to elucidate all transition state structures. This ONIOM method approach has been successfully used to identify the nature of enzymatic reactions, describing both transition and intermediate structures along the reaction pathways.[38-42]

4.3 Results And Discussion

4.3.1 The Protonation State of His504's Imidazole

The protonation state of His504 will dictate the ring opening mechanism of GlmS with its imidazole potentially acting as a base or an acid to initiate the reaction. Previously it has been proposed that His504 acts as a base. Its imidazole must sit in its neutral form to abstract the proton of the O2 hydroxyl of Fru-6-P. In order to understand His504's role in on the ring opening mechanism two protonation states of His504 were assigned for molecular dynamics simulation. The root-mean squared deviation (RMSD) of all atoms, relative to their initial crystal structure, within ~12 Å of Fru-6-P were measured for each case (Figure 4.1).

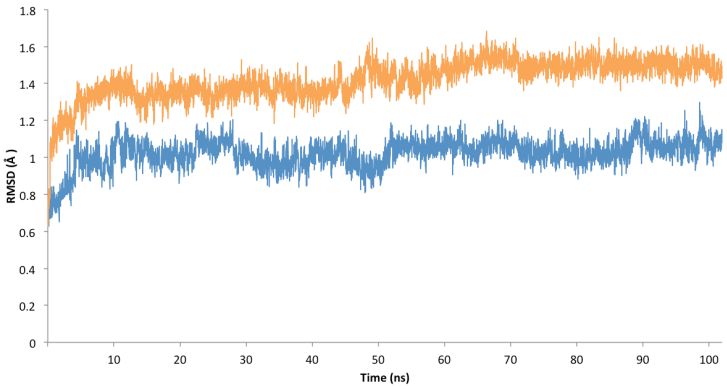

Figure 4.1. A RMSD plot of all atoms within ~12 Å of Fru-6-P relative to their crystal structure over a 100ns production run with His504 protonated in blue and His504 neutral in orange.

Interestingly, the protonated His504 model shows a narrow range of ~0.8 to ~1.2 Å over the 100 ns production run normalizing at ~1.0 Å. This suggests that with His504 in its protonated form, the active site of GlmS has similar positioning of its atoms relative to its crystal structure. Conversely, the neutral His504 model shows a

larger range from ~1.2 to ~1.6 Å, normalizing at ~1.4 Å, suggesting a greater deviation from the reference crystal structure positions.

A distance plot was constructed measuring the distance between His504's nitrogen to Fru-6-P's ether oxygen (Figure 4.2). Over the course of the 100ns production run, the neutral His504 fluctuates widely from ~3.3 Å to ~6.2 Å, normalizing at an average distance of ~4.2 Å. Conversely, the protonated form shows a much narrower range ~2.7 Å to ~4.8 Å normalizing at an average distance ~3.0 Å.

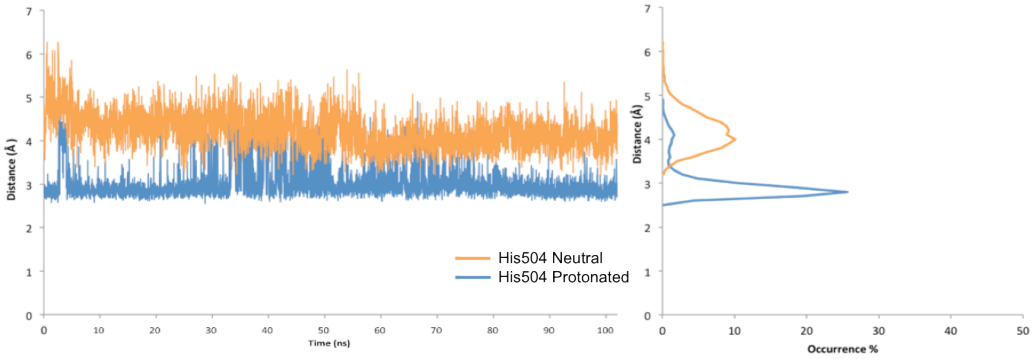

Figure 4.2. A distance plot of $_{His504}N\cdots O_{Fru\text{-}6\text{-}P}$ over a 100ns production run with His504 protonated in blue and His504 neutral in orange. The chart on the right shows the occurrence of each distance as a percentage.

Two representative structures were chosen from the MD simulations, showcasing the active site geometry for the protonated His504 model as well as for the neutral model. The structures contain the substrate and His504's interactions as well as the residues associated with phosphate binding. The representative structures are displayed in Figure 4.3.

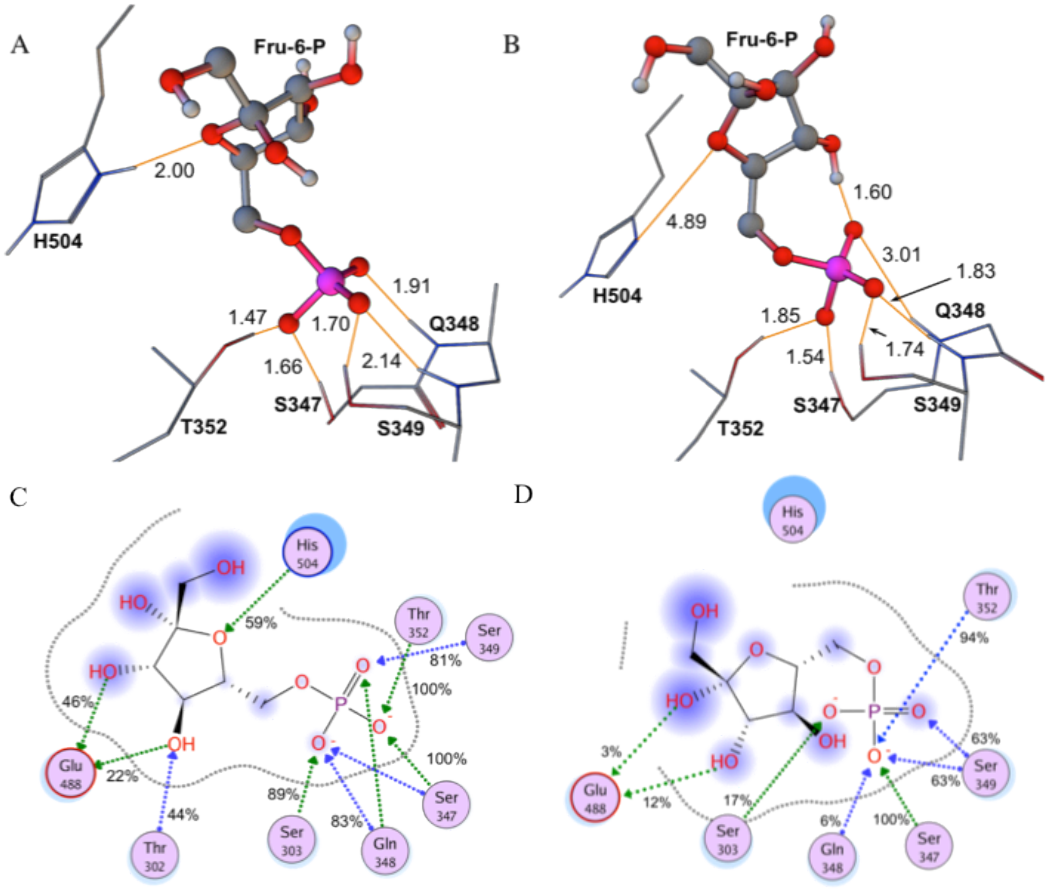

Figure 4.3. Representative structures selected from a 100 ns production run (see Computational Details) with His504 (A) protonated and (B) neutral, distances in Ångstrom. Ligand interaction diagrams showcasing percentage of interactions over the simulation are also shown for the His504 (C) protonated and (D) neutral.

As shown, there are clear differences between the active sites, mainly in the positioning of His504. When His504 sits in its neutral state it appears to have shifted away from Fru-6-P and, in fact, the hydroxyl's proton that it is expected to abstract is 6.82 Å away. The hydroxyl itself has rotated away from the imidazole of His504 and appears to share a hydrogen bond with a nearby peptide backbone (not shown). Over the course of the MD production run, the distance between the

hydroxyl and the imidazole nitrogen fluctuated between ~4.9 Å to ~8.5 Å with an average distance of ~6.7 Å (Figure 4.4).

Interestingly, the phosphate-binding region was affected as shown in the ligand interaction diagrams (Figure 4.3C & 4.3D). Most of the hydrogen bond network remains consistent between the two models. Thr352, Ser347, and Ser349 hydrogen bonds fluctuate slightly from each other, showing small variances of less than ~0.2 to ~0.3 Å. One large difference between the models arises from the hydrogen bond of Gln348's amide peptide bond and Ser303's hydroxyl. In the protonated model, the Gln348 hydrogen bond shows a distance of ~1.9 Å while in the neutral model the distance is ~3.0 Å. In fact, in the neutral model, the percentage of interaction for Gln348 dropped dramatically from 83% to 6%. Ser303's interaction was also largely affected showing a drop from 89% to 17%.

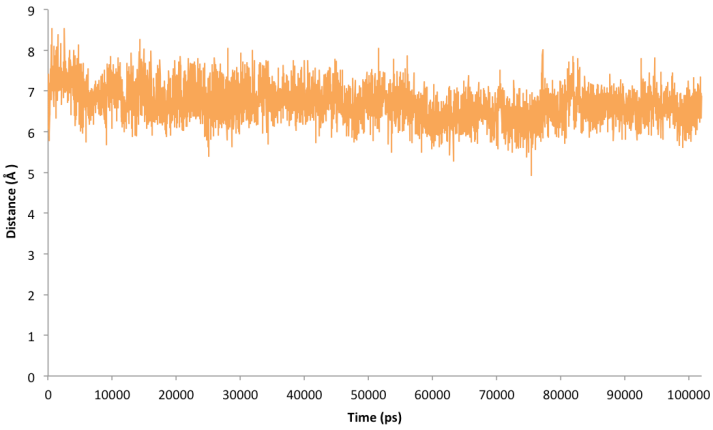

Figure 4.4. A distance plot of $_{His504}N\cdots HO\text{-}_{Fru\text{-}6\text{-}P}$ over a 100ns production run with His504 neutral.

Most importantly, the two structures highlight an interesting role for His504 in the ring opening mechanism. The protonated state forms a hydrogen bond with the ether oxygen of Fru-6-P at ~2.0 Å. This distance remains fairly consistent during the

course of the MD simulation showing a percentage of interaction of 59%. This strongly suggests that His504 may act as a proton donor during the ring opening mechanism, similar to glucosamine-6-phosphate deaminase. Furthermore, the neutral form sits at a relatively long distance, ~6.8 Å, to act as a proton acceptor to Fru-6-P's hydroxyl. It would be expected that this distance would be shorter and more consistent given that the proposed mechanism suggests His504's imidazole acting as a base (Scheme 4.1). In fact, the percentage of interaction shows the neutral His504 residue having no interaction with the ligand over the course of the 100ns run.

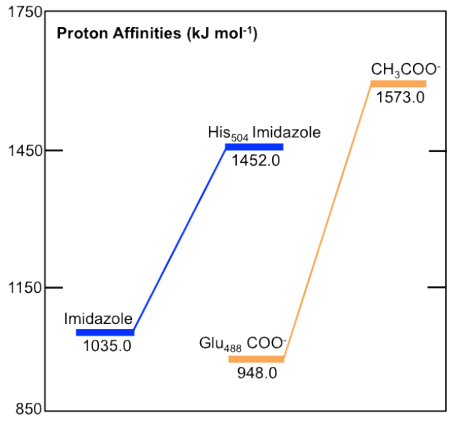

Figure 4.5. Calculated proton affinities of His504's imidazole and Glu488's carboxyl compared to their molecular equivalents. The calculated proton affinity of water is 745.6 kJ mol^{-1}.

To gain further insights on the preferred protonation state of His504, we performed a proton affinity analysis on both His504 and Glu488. PROPKA results suggested His504 would be in its neutral state, however the MD results suggested otherwise. A protonated His504 promotes the preferred geometry to act as a proton donor during the ring opening mechanism. The neutral form of His504 did not show hydrogen bonding with the expected hydroxyl oxygen it is proposed to abstract. The

proton affinities for both His504 and Glu488 in Figure 4.5 show that His504's imidazole prefers to be in its protonated form while Glu488's carboxyl prefers its neutral form.

4.3.2 The Ring Opening Mechanism Initiated by His504

Due to the structural similarities that GlmS shares with glucosamine 6-phosphate deaminase, we explored the effects of His504 acting as the sole catalytic residue, that is, it acting initially as a proton donor and later as a proton acceptor. The optimized **RC$_{(His)}$** placed His504's hydrogen at a distance of 1.77 Å from Fru-6-P's ether oxygen bond which shows a distance of 1.45 Å in Figure 4.6.

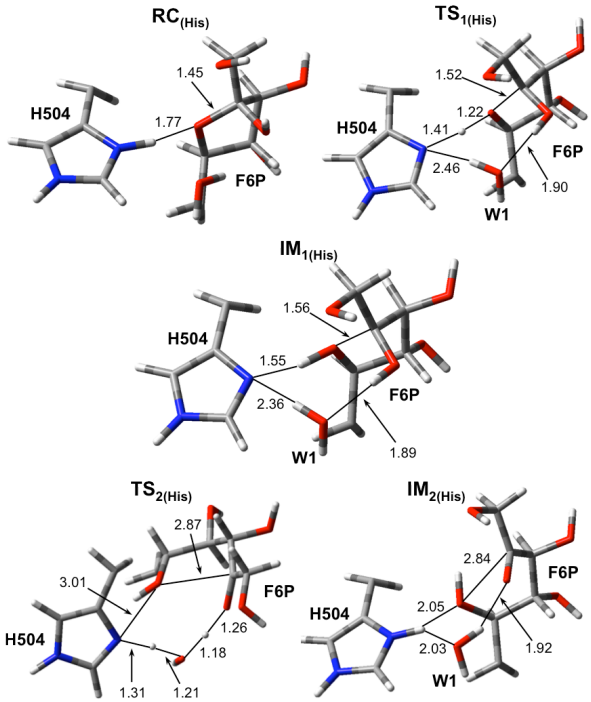

Figure 4.6. Optimized structures of the reactant complex (**RC$_{(His)}$**), intermediates (**IM$_{(His)}$**), and transition structures (**TS$_{(His)}$**) of the ring opening mechanism catalyzed by His504, highlighting key residues and relevant distances in Ångstrom.

The reaction begins with His504 donating its proton to the ether oxygen, proceeding through **TS1$_{(His)}$** with a potential energy barrier of 72.7 kJ mol^{-1} relative to **RC$_{(His)}$** (Figure 4.7). The C2-O ether bond lengthens to a distance of 1.52 Å while a nearby water molecule (W1) rotates to hydrogen bond with His504 at a distance of 2.46 Å. Interestingly, the C2 hydroxyl, that is expected to form the carbonyl once the ring has opened, has rotated to form a hydrogen bond with W1's oxygen at a distance of 1.90 Å.

IM1$_{(His)}$ forms with a relative energy of 69.9 kJ mol^{-1} where the ether bond has lengthened to 1.56 Å. The newly formed oxonium ion is hydrogen bonded to His504's nitrogen, while W1 and the C2 hydroxyl forms a hydrogen bond network in a geometry capable of proton shuttling. Indeed, the proton shuttle occurs along **TS2$_{(His)}$** with a relative energy of 107.2 kJ mol^{-1}.

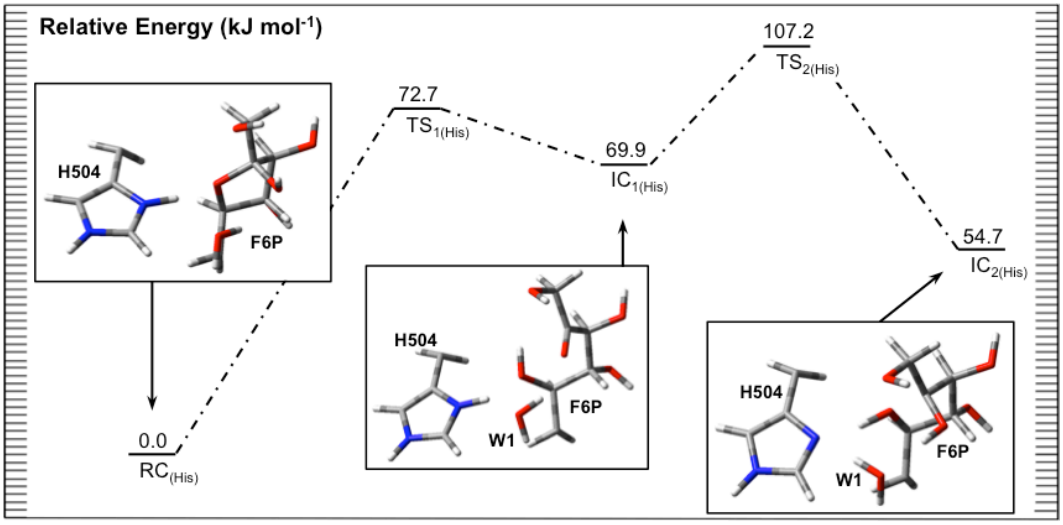

Figure 4.7. Potential energy surface obtained for the ring opening mechanism catalyzed by His504, see Computational Details.

Finally, the ring is opened in **IM2$_{(His)}$** which has a potential energy of 54.7 kJ mol^{-1} relative to **RC$_{(His)}$**. The ether bond has broken, with the atoms 2.84 Å away from each

other. The protonated N3 of His504 shows a distance of 2.03 Å to W1 and 2.05 Å to the newly protonated oxygen of Fru-6-P. W1 also maintains its hydrogen bond with the carbonyl oxygen at a distance of 1.92 Å.

4.3.3 The Ring Opening Mechanism Initiated by Glu488

The initial **RC$_{(His/Glu)}$** optimized from the MD production run showed Glu488 in its deprotonated state as calculated by the proton affinities, but also showed its geometry in agreement to act as a base during the ring opening mechanism (Figure 4.8). The **RC$_{(His/Glu)}$** places one of the carboxyl oxygen atoms of Glu488 at a distance of 1.70 Å from the C3 hydroxyl of Fru-6-P. Moreover, this promoted the C2 hydroxyl's proton, the one expected to form the carbonyl, to share a hydrogen bond with the C3 hydroxyl at a distance of 2.27 Å. This provided an environment where a proton shuttle could occur across the substituent hydroxyls to the carboxyl oxygen of Glu488. The interaction diagram of Glu488 shows a relatively consistent interaction with the C3 hydroxyl of Fru-6-P at 46% occurrence, Figure 4.3C. Therefore the ring opening mechanism catalyzed by Glu488 was considered.

Glu488 abstracts the proton from the C3 hydroxyl to form **TS1$_{(His/Glu)}$** with a potential energy barrier of 70.0 kJ mol^{-1} relative to the **RC$_{(His/Glu)}$** (Figure 4.9). As shown in Figure 4.8, **TS1$_{(His/Glu)}$** begins to form an oxyanion. Two water molecules (W1 and W2 in Figure 4.8) form hydrogen bonds with the incipient oxyanion at a distance of 1.97 Å and 2.12 Å, respectively. Interestingly, the hydrogen bond shared between the C3 hydroxyl has increased in distance from 2.27 Å in the **RC$_{(His/Glu)}$** to 2.36 Å in **TS1$_{(His/Glu)}$**; however in **IM1$_{(His/Glu)}$** this bond returns to relatively the same distance at 2.26 Å. **IM1$_{(His/Glu)}$** has a relative energy of 59.6 kJ mol^{-1}, forming a stable oxyanion intermediate that is stabilized through W1, W2 and the C3 hydroxyl. The hydrogen bonds shared with W1 and W2 during the **TS1$_{(His/Glu)}$** formation shorten

at a distance of 1.95 Å and 1.88 Å, respectively. A hydrogen bond with Glu488's newly formed carboxylic acid further stabilizes the oxyanion at a distance of 1.81 Å.

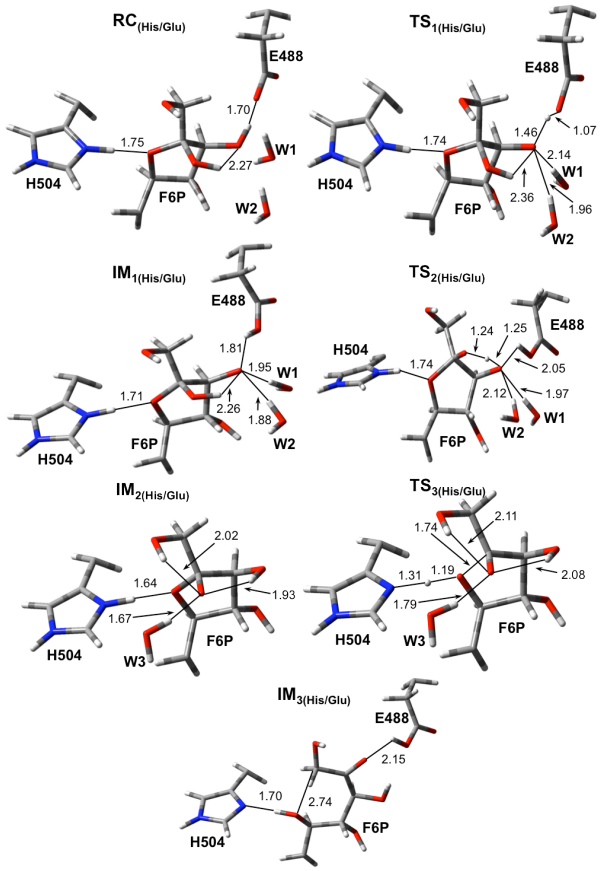

Figure 4.8. Optimized structures of the reactant complex (**RC$_{(His/Glu)}$**), intermediates (**IM$_{(His/Glu)}$**), and transition structures (**TS$_{(His/Glu)}$**) of the ring opening mechanism catalyzed by Glu488 and His504, highlighting key residues and relevant distances in Ångstrom.

The reaction proceeds through **TS2$_{(His/Glu)}$** where the C2 hydroxyl's hydrogen is deprotonated by the newly formed C3 oxyanion in **IM1$_{(His/Glu)}$** with a relative energy barrier of 91.5 kJ mol^{-1}. In **TS2$_{(His/Glu)}$** the proton is 1.25 Å away from the oxyanion. A newly formed oxyanion appears in **IM2$_{(His/Glu)}$** stabilized by hydrogen bonding to the C1 and C3's hydroxyl's hydrogens at a distance of 2.02 Å and 1.93 Å,

respectively, as well as a water molecule (W3 in Figure 4.8) at a distance of 1.67 Å. His504 has moved closer to the ether oxygen of Fru-6-P when compared to the **RC(His/Glu)**, moving from 1.75 Å to 1.64 Å. This produced a potential energy of 39.3 kJ mol^{-1} relative to the **RC(His/Glu)**.

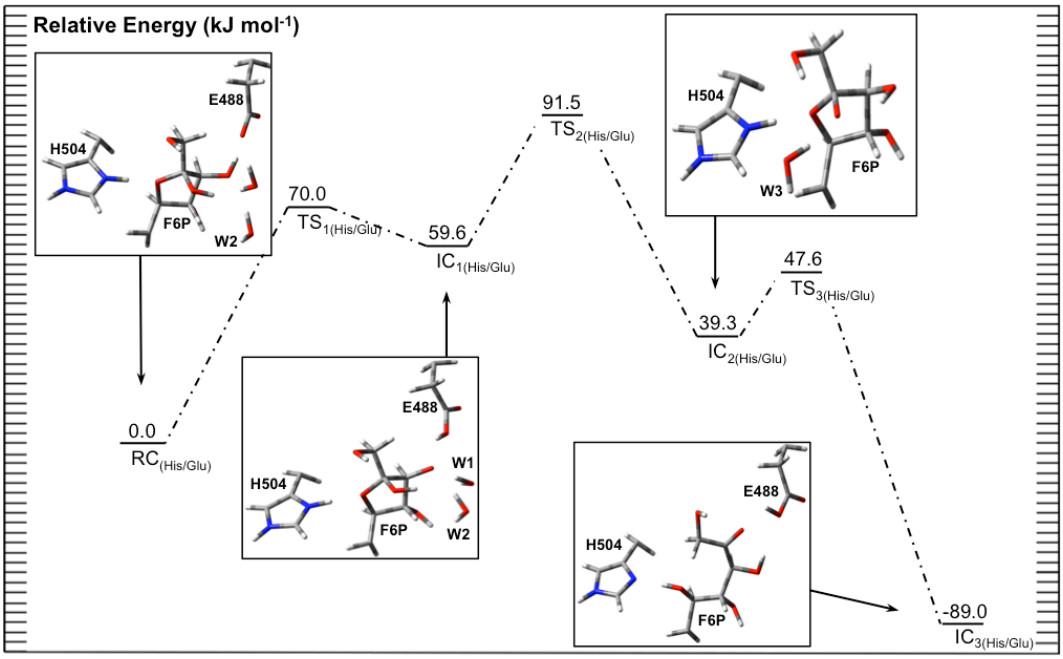

Figure 4.9. Potential energy surface obtained for the ring opening mechanism catalyzed by Glu488 and His504, see Computational Details.

Finally, the ring begins to open as His504 begins to donate its proton to the ether oxygen of Fru-6-P in **TS3(His/Glu)** producing a relative energy difference of 47.6 kJ mol^{-1} with respect to **RC(His/Glu)**. The proton is distanced at 1.19 Å from the ether oxygen as it moves away from the incipient carbonyl at a distance of 1.74 Å with respect to the carbon. The C2 oxygen remains stabilized by the C1 and C3 hydroxyl's at a distance of 2.11 and 2.08 Å, respectively, while W3's hydrogen bond is distanced at 1.79 Å.

The Fru-6-P open structure, **IM3$_{(His/Glu)}$**, has a relative energy of -89.0 kJ mol^{-1} with respect to **RC$_{(His/Glu)}$**. The newly formed C5 hydroxyl, previously the ether oxygen, is 2.74 Å from the carbonyl's carbon atom, while it shares a hydrogen bond with His504 at a distance of 1.70 Å. Glu488 further stabilizes the newly formed intermediate sharing a hydrogen bond with the carbonyl oxygen at a distance of 2.15 Å.

4.4 Conclusion

In the present study, we have taken a complimentary approach to outlining glucosamine-6-phosphate synthase catalytic ring opening mechanism through the use of molecular dynamics and QM/MM models. Previously, the mechanism proposed His504 acting as the sole residue responsible for the ring opening mechanism acting as both the proton acceptor and donator, however our results suggest an alternative pathway may occur.

The molecular dynamic simulations performed show that when His504 is in its neutral state the geometry and distance relative to the substrate is affected. The hydroxyl it is expected to deprotonate sits at an average distance of ~6.7 Å away throughout the 100 ns run. Alternatively, the molecular dynamic simulations show that when His504 is protonated it sits at a distance of ~3.0 Å from the ether oxygen of Fru-6-P, maintaining a consistent hydrogen bond. Interestingly, our proton affinity calculations show that His504 prefers to be in its protonated state in the reactive complex.

The catalytic ring opening mechanism was further explored with a QM/MM approach. The ring opens with a cooperative effort between His504 and Glu488. A stepwise proton shuttle occurs across the substituent's hydroxyls as Glu488 initiates the reaction through proton abstraction from the C3 O-H group. This led to a potential energy barrier of 91.5 kJ mol^{-1} along the reaction pathway. Conversely,

we investigated His504 acting as the sole catalytic residue, initiating the ring opening by donating its proton to the ether oxygen. This reaction followed a stepwise mechanism giving a potential energy barrier of 107.2 kJ mol^{-1}.

4.5 References

(1) Ghosh, S.; Blumenthal, H. J.; Davidson, E.; Roseman, S. Glucosamine metabolism. V. Enzymatic synthesis of glucosamine 6-phosphate. *J. Biol. Chem.* **1960**, *235*, 1265.

(2) Whelan, W. L.; Ballou, C. E. Sporulation in D-glucosamine auxotrophs of Saccharomyces cerevisiae: meiosis with defective ascospore wall formation. *J. Bacteriol.* **1975**, *124*, 1545.

(3) Imada, A.; Nozaki, Y.; Kawashima, F.; Yoneda, M. Regulation of glucosamine utilization in Staphylococcus aureus and Escherichia coli. *J. Gen. Microbiol.* **1977**, *100*, 329.

(4) Wojciechowski, M.; Milewski, S.; Mazerski, J.; Borowski, E. Glucosamine-6-phosphate synthase, a novel target for antifungal agents. Molecular modelling studies in drug design. *Acta. Biochim. Pol.* **2005**, *52*, 647.

(5) Moraes, G. L.; Gomes, G. C.; de Sousa, P. R. M.; Alves, C. N.; Govender, T.; Kruger, H. G.; Maguire, G. E. M.; Lamichhane, G.; Lameira, J. Structural and functional features of enzymes of Mycobacterium tuberculosis peptidoglycan biosynthesis as targets for drug development. *Tuberculosis* **2015**, *95*, 95.

(6) Kaneto, H.; Xu, G.; Song, K. H.; Suzuma, K.; Bonner-Weir, S.; Sharma, A.; Weir, G. C. Activation of the hexosamine pathway leads to deterioration of pancreatic beta-cell function through the induction of oxidative stress. *J. Biol. Chem.* **2001**, *276*, 31099.

(7) Tang, J.; Neidigh, J. L.; Cooksey, R. C.; McClain, D. A. Transgenic mice with increased hexosamine flux specifically targeted to beta-cells exhibit hyperinsulinemia and peripheral insulin resistance. *Diabetes* **2000**, *49*, 1492.

(8) Wu, G.; Haynes, T. E.; Yan, W.; Meininger, C. J. Presence of glutamine:fructose-6-phosphate amidotransferase for glucosamine-6-phosphate

synthesis in endothelial cells: effects of hyperglycaemia and glutamine. *Diabetologia* **2001**, *44*, 196.

(9) Massiere, F.; Badet-Denisot, M. A. The mechanism of glutamine-dependent amidotransferases. *Cell Mol. Life Sci.* **1998**, *54*, 205.

(10) Raushel, F. M.; Thoden, J. B.; Holden, H. M. The amidotransferase family of enzymes: molecular machines for the production and delivery of ammonia. *Biochem.* **1999**, *38*, 7891.

(11) Zalkin, H. The amidotransferases. *Adv. Enzymol. Relat. Areas Mol. Biol.* **1993**, *66*, 203.

(12) Badet, B.; Vermoote, P.; Haumont, P. Y.; Lederer, F.; LeGoffic, F. Glucosamine synthetase from Escherichia coli: purification, properties, and glutamine-utilizing site location. *Biochem.* **1987**, *26*, 1940.

(13) Mouilleron, S.; Badet-Denisot, M. A.; Golinelli-Pimpaneau, B. Glutamine binding opens the ammonia channel and activates glucosamine-6P synthase. *J. Biol. Chem.* **2006**, *281*, 4404.

(14) Leriche, C.; BadetDenisot, M. A.; Badet, B. Characterization of a phosphoglucose isomerase-like activity associated with the carboxy-terminal domain of Escherichia coli glucosamine-6-phosphate synthase. *J. Am. Chem. Soc.* **1996**, *118*, 1797.

(15) Milewski, S. Glucosamine-6-phosphate synthase-the multi-facets enzyme. *Bba-Protein. Struct. M.* **2002**, *1597*, 173.

(16) Durand, P.; Golinelli-Pimpaneau, B.; Mouilleron, S.; Badet, B.; Badet-Denisot, M. A. Highlights of glucosamine-6P synthase catalysis. *Arch. Bioch. Biophys.* **2008**, *474*, 302.

(17) Teplyakov, A.; Obmolova, G.; Badet, B.; Badet-Denisot, M. A. Channeling of ammonia in glucosamine-6-phosphate synthase. *J. Mol. Biol.* **2001**, *313*, 1093.

(18) Mouilleron, S.; Badet-Denisot, M. A.; Badet, B.; Golinelli-Pimpaneau, B. Dynamics of glucosamine-6-phosphate synthase catalysis. *Arch. Bioch. Biophys.* **2011**, *505*, 1.

(19) Milewski, S.; Janiak, A.; Wojciechowski, M. Structural analogues of reactive intermediates as inhibitors of glucosamine-6-phosphate synthase and phosphoglucose isomerase. *Arch. Bioch. Biophys.* **2006**, *450*, 39.

(20) Teplyakov, A.; Obmolova, G.; Badet-Denisot, M. A.; Badet, B.; Polikarpov, I. Involvement of the C terminus in intramolecular nitrogen channeling in glucosamine 6-phosphate synthase: evidence from a 1.6 A crystal structure of the isomerase domain. *Structure* **1998**, *6*, 1047.

(21) Zhao, Y.; Chen, N.; Wu, R.; Cao, Z. A QM/MM MD study of the pH-dependent ring-opening catalysis and lid motif flexibility in glucosamine 6-phosphate deaminase. *Phys. Chem. Chem. Phys.* **2014**, *16*, 18406.

(22) Montero-Moran, G. M.; Lara-Gonzalez, S.; Alvarez-Anorve, L. I.; Plumbridge, J. A.; Calcagno, M. L. On the multiple functional roles of the active site histidine in catalysis and allosteric regulation of Escherichia coli glucosamine 6-phosphate deaminase. *Biochem.* **2001**, *40*, 10187.

(23) Solomons, J. T.; Zimmerly, E. M.; Burns, S.; Krishnamurthy, N.; Swan, M. K.; Krings, S.; Muirhead, H.; Chirgwin, J.; Davies, C. The crystal structure of mouse phosphoglucose isomerase at 1.6A resolution and its complex with glucose 6-phosphate reveals the catalytic mechanism of sugar ring opening. *J. Mol. Biol.* **2004**, *342*, 847.

(24) Rostkowski, M.; Olsson, M. H. M.; Sondergaard, C. R.; Jensen, J. H. Graphical analysis of pH-dependent properties of proteins predicted using PROPKA. *BMC Struct. Biol.* **2011**, *11*.

(25) Olsson, M. H. M.; Sondergaard, C. R.; Rostkowski, M.; Jensen, J. H. PROPKA3: Consistent Treatment of Internal and Surface Residues in Empirical pK(a) Predictions. *J. Chem. Theory Comput.* **2011**, *7*, 525.

(26) Case, D. A.; Berryman, J. T.; Betz, R. M.; Cerutti, D. S.; Cheatham, III, T. E.; Darden, T. A.; Duke, R. E.; Giese, T. J.; Gohlke, H.; Goetz, A. W.; Homeyer, N.; Izadi, S.; Janowski, P.; Kaus, J.; Kovalenko, A.; Lee, T. S.; LeGrand, S.; Li, P.; Lin, C.; Luchko, T.; Luo, R.; Madej, B.; Merz, K. M.; Monard, G.; Needham, P.; Nguyen, H.; Nguyen, H. T.; Omelyan, I.; Onufriev, A.; Roe, D. R.; Roitberg, A.; Salomon-Ferrer, R.; Simmerling, C. L.; Smith, W.; Swails, J.; Walker, R. C.; Wang, J.; Wolf, R. M.; Wu, X.; York D. M.; Kollman, P. A. (2015), AMBER 2015, University of California, San Francisco.

(27) Jorgensen, W. L.; Chandrasekhar, J.; Madura, J. D.; Impey, R. W.; Klein, M. L. Comparison of Simple Potential Functions for Simulating Liquid Water. *J. Chem. Phys.* **1983**, *79*, 926.

(28) Salomon-Ferrer, R.; Gotz, A. W.; Poole, D.; Le Grand, S.; Walker, R. C. Routine Microsecond Molecular Dynamics Simulations with AMBER on GPUs. 2. Explicit Solvent Particle Mesh Ewald. *J. Chem. Theory Comput.* **2013**, *9*, 3878.

(29) Goetz, A. W.; Williamson, M. J.; Xu, D.; Poole, D.; Le Grand, S.; Walker, R. C. Routine Microsecond Molecular Dynamics Simulations with AMBER on GPUs. 1. Generalized Born. *J. Chem. Theory Comput.* **2012**, *8*, 1542.

(30) Maier, J. A.; Martinez, C.; Kasavajhala, K.; Wickstrom, L.; Hauser, K. E.; Simmerling, C. ff14SB: Improving the Accuracy of Protein Side Chain and Backbone Parameters from ff99SB. *J. Chem. Theory Comput.* **2015**, *11*, 3696.

(31) Wang, J.; Wang, W.; Kollman, P. A.; Case, D. A. Automatic atom type and bond type perception in molecular mechanical calculations. *J. Mol. Graph. Model.* **2006**, *25*, 247.

(32) Wang, J.; Wolf, R. M.; Caldwell, J. W.; Kollman, P. A.; Case, D. A. Development and testing of a general amber force field. *J. Comput. Chem.* **2004**, *25*, 1157.

(33) Frisch, M. J.; Trucks, G. W.; Schlegel, H. B.; Scuseria, G. E.; Robb, M. A.; Cheeseman, J. R.; Scalmani, G.; Barone, V.; Mennucci, B.; Petersson, G. A.; Nakatsuji, H.; Caricato, M.; Li, X.; Hratchian, H. P.; Izmaylov, A. F.; Bloino, J.; Zheng, G.; Sonnenberg, J. L.; Hada, M.; Ehara, M.; Toyota, K.; Fukuda, R.; Hasegawa, J.; Ishida, M.; Nakajima, T.; Honda, Y.; Kitao, O.; Nakai, H.; Vreven, T.; Montgomery, J., J. A. ; Peralta, J. E.; Ogliaro, F.; Bearpark, M.; Heyd, J. J.; Brothers, E.; Kudin, K. N.; Staroverov, V. N.; Kobayashi, R.; Normand, J.; Raghavachari, K.; Rendell, A.; Burant, J. C.; Iyengar, S. S.; Tomasi, J.; Cossi, M.; Rega, N.; Millam, J. M.; Klene, M.; Knox, J. E.; Cross, J. B.; Bakken, V.; Adamo, C.; Jaramillo, J.; Gomperts, R.; Stratmann, R. E.; Yazyev, O.; Austin, A. J.; Cammi, R. P., C.; Ochterski, J. W.; Martin, R. L.; Morokuma, K.; Zakrzewski, V. G.; Voth, G. A.; Salvador, P.; Dannenberg, J. J.; Dapprich, S.; Daniels, A. D.; Farkas, Ö.; Foresman, J. B.; Ortiz, J. V.; Cioslowski, J. Fox, D. J. Gaussian 09, Gaussian, Inc., CT, Wallingford 2009

(34) Andersen, H. C. Molecular-Dynamics Simulations at Constant Pressure and-or Temperature. *J. Chem. Phys.* **1980**, *72*, 2384.

(35) Vreven, T.; Byun, K. S.; Komaromi, I.; Dapprich, S.; Montgomery, J. A.; Morokuma, K.; Frisch, M. J. Combining quantum mechanical methods with molecular mechanics methods in ONIOM. *Abstr. Pap. Am. Chem. S.* **2006**, *232*, 408.

(36) Chung, L. W.; Sameera, W. M. C.; Ramozzi, R.; Page, A. J.; Hatanaka, M.; Petrova, G. P.; Harris, T. V.; Li, X.; Ke, Z. F.; Liu, F. Y.; Li, H. B.; Ding, L. N.; Morokuma, K. The ONIOM Method and Its Applications. *Chem. Rev.* **2015**, *115*, 5678.

(37) Becke, A. D. Density-Functional Thermochemistry .3. The Role of Exact Exchange. *J. Chem. Phys.* **1993**, *98*, 5648.

(38) Gherib, R.; Dokainish, H. M.; Gauld, J. W. Multi-scale computational enzymology: enhancing our understanding of enzymatic catalysis. *Int. J. Mol. Sci.* **2014**, *15*, 401.

(39) Hermann, J. C.; Pradon, J.; Harvey, J. N.; Mulholland, A. J. High Level QM/MM Modeling of the Formation of the Tetrahedral Intermediate in the Acylation of Wild Type and K73A Mutant TEM-1 Class A beta-Lactamase. *J. Phys. Chem. A* **2009**, *113*, 11984.

(40) Stanton, C. L.; Kuo, I. F. W.; Mundy, C. J.; Laino, T.; Houk, K. N. QM/MM metadynamics study of the direct decarboxylation mechanism for orotidine-5 '-monophosphate decarboxylase using two different QM regions: Acceleration too small to explain rate of enzyme catalysis. *J. Phys. Chem. B* **2007**, *111*, 12573.

(41) Pinto, G. P.; Bras, N. F.; Perez, M. A. S.; Fernandes, P. A.; Russo, N.; Ramos, M. J.; Toscano, M. Establishing the Catalytic Mechanism of Human Pancreatic alpha-Amylase with QM/MM Methods. *J. Chem. Theory Comput.* **2015**, *11*, 2508.

(42) Huang, W.; Gauld, J. W. Tautomerization in the UDP-galactopyranose mutase mechanism: a DFT-cluster and QM/MM investigation. *J. Phys. Chem. B* **2012**, *116*, 14040.

Chapter 5:
Conclusions

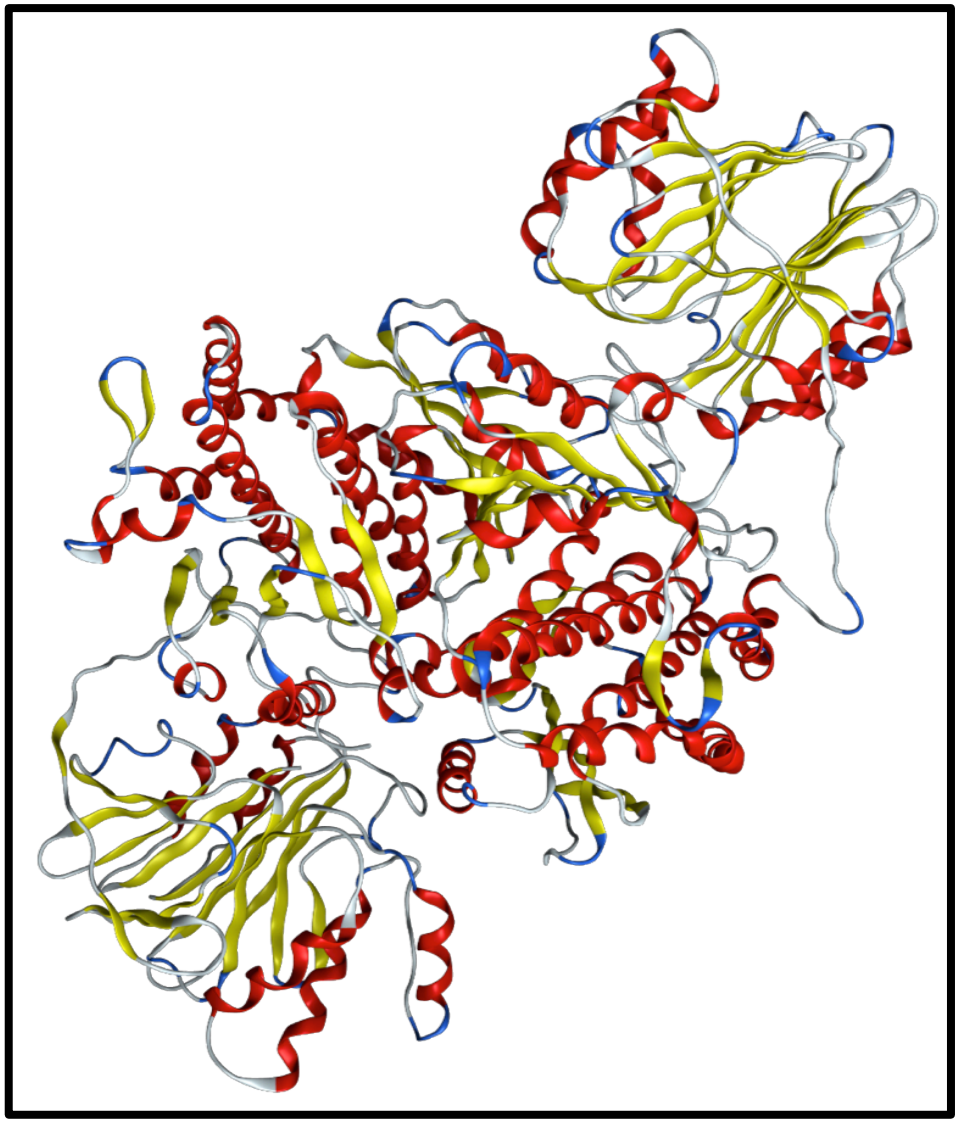

5.1 Conclusions

In this thesis, a multifaceted computational approach was taken to explore two enzymatic systems involved in ring opening mechanisms. The mechanism of inhibition of a β-lactamase inhibitor was explored and the ring opening mechanism of glucosamine 6-P synthase's substrate fructose-6-phosphate was also identified.

In chapter 3, the inhibition of CTX-M β-lactamase was explored with the inhibitor tazobactam. Several approaches were taken to explore the nuances of the enzyme's hydrolytic activity including molecular dynamic simulations and quantum mechanics/molecular mechanics (QM/MM) models. In particular, the formation of the bridging intermediate between Ser70 and Ser130 was elucidated. Previously, the proposed mechanism stated that Ser130's involvement in the reaction was primarily a result of Lys73's hydrogen bonding.[1] Specifically, if Lys73 shared a hydrogen bond with Ser130, the bridging intermediate would not form. Our results show that Ser130's involvement is independent of Lys73's interactions during the reaction complex. Moreover, once Ser70's covalent attachment has occurred, and the intermediate complex is formed, the dynamics of the enzyme play an important role. The dynamics of the intermediate complex allows for Ser130's proper orientation where it is deprotonated by Lys73 allowing for its nucleophilic attack ultimately forming the bridge intermediate. The structure and positioning of acylated intermediate should be taken into consideration for future inhibitor design with the potential of designing one that promotes the bridging intermediate formation. We also explored the consequences of the various protonation states of the catalytic residues and have identified that each scenario leads to a neutral Lys73, allowing it to be readily available for Ser130's deprotonation.

In chapter 4, the synthase site of glucosamine-6-phosphate synthase was explored through long time scale molecular dynamics simulations, quantum mechanical clusters, and quantum mechanics/molecular mechanics models. Current

literature has suggested the catalytic ring opening mechanism of fructose-6-phosphate occurred through a neutral His504 residue.[2] Specifically, His504 is proposed to act initially as the base for deprotonation of the C2-OH. Our results indicate that the neutral His504 shows no interaction with the substrate during a 100ns molecular dynamic simulation. We have also shown that this residue in particular prefers to be in its protonated state as indicated by both the calculated proton affinities and its overall of interaction with the substrate during simulations. The role of His504 was further highlighted as we explored the reaction coordinate of the ring opening mechanism. While the protonated His504 shows a feasible energy barrier, an alternative mechanism was explored involving a concerted effort between Glu488 and His504. Our results indicate that the reaction proceeds through a stepwise fashion with the reaction being initiated by Glu488 through proton abstraction of fructose-6- phosphate's C3 hydroxyl. This ultimately leads to His504's involvement by protonation to the ether oxygen of fructose-6-phosphate.

The work in this thesis highlights the significance of taking a multi-faceted computational approach. Severe limitations would arise if restricted to a specific technique. By approaching enzymatic systems through molecular dynamics and quantum mechanics/molecular mechanics, the pitfalls of one method can be compensated by the other. The combination allows for deeper insights into the behaviour of enzymes. Future studies should strongly consider this approach when exploring enzymes.

5.2 References

(1) Heidari-Torkabadi, H.; Bethel, C. R.; Ding, Z.; Pusztai-Carey, M.; Bonnet, R.; Bonomo, R. A.; Carey, P. R. "Mind the Gap": Raman Evidence for Rapid Inactivation of CTX-M-9 beta-Lactamase Using Mechanism-Based Inhibitors that Bridge the Active Site. *J. Am. Chem. Soc.* **2015**, *137*, 12760.

(2) Mouilleron, S.; Badet-Denisot, M. A.; Badet, B.; Golinelli-Pimpaneau, B. Dynamics of glucosamine-6-phosphate synthase catalysis. *Arch. Bioch. Biophys.* **2011**, *505*, 1.

Chapter 6:
Future Work

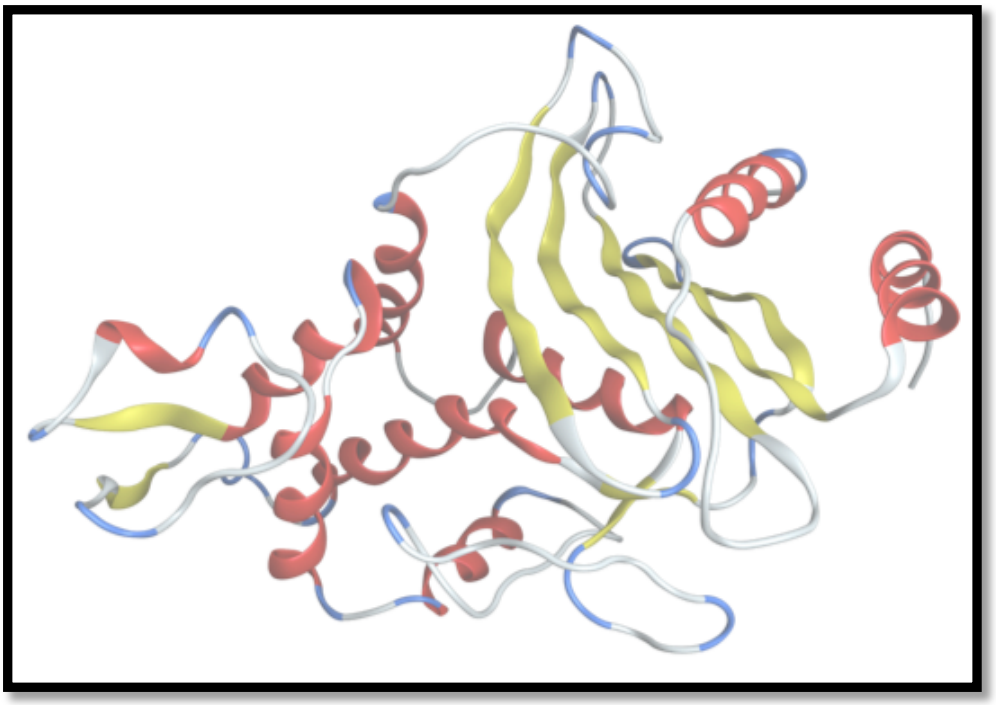

6.1 Future Work

While many insights were gained for both β-lactamase and glucosamine-6-phosphate synthase, the formation of the last intermediate step for the β-lactamase study requires more investigation. Particular insights were gained on the consequences of the S130G mutant and the various protonation states; the dissociation of the amine bond has yet to be determined.

The bridged intermediate has a double bond between the bridging carbons; however the pathway we explored shows no double bond characteristic.[1] Moreover, the leaving nitrogen would require protonation in order to be a better leaving group. This would also lead to promotion of Ser130's oxygen attacking the expected carbon. Herein we propose two alternative reaction schemes, which may lead to a favourable pathway for the bridging intermediate formation (Scheme 6.1).

Scheme 6.1. Proposed reaction pathway of cross-linked species formation with tazobactam with (A) sulfinate acting as the acid/base catalyst and (B) carboxylate acting as the acid/base catalyst.

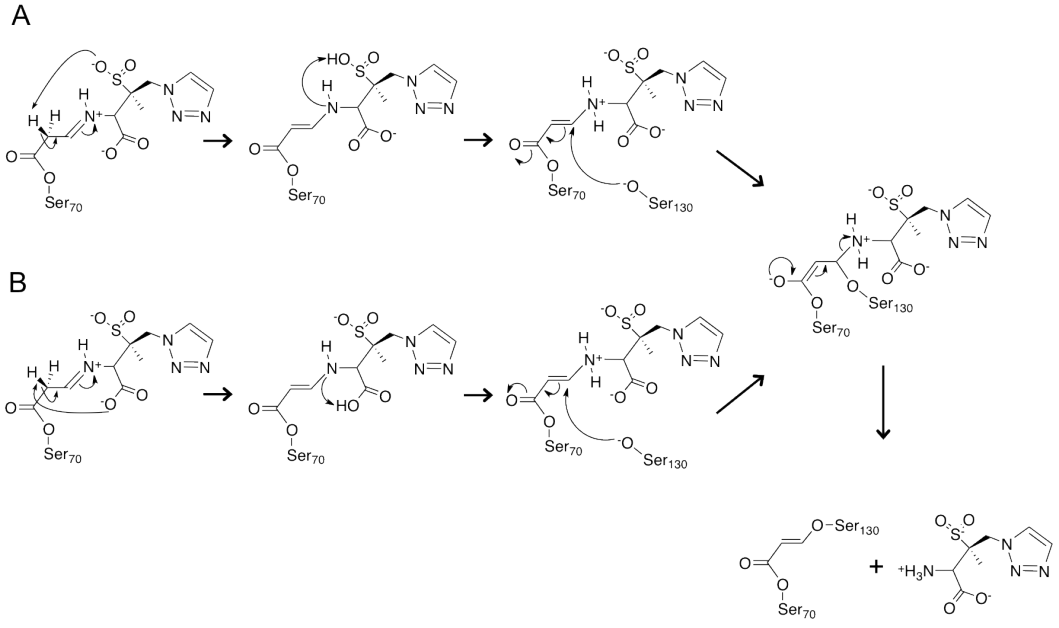

Substrate's functional groups may act as a base during reactions.[2] We propose a similar pathway for the formation of the bridging intermediate. In the first proposed mechanism, we suggest that a carbon is deprotonated by the nearby substrate's carboxylate, then the nitrogen is protonated by either the solvent front or *via* the same carboxylic acid. This leads to a protonated amine that leads to Ser130's attack. The bond dissociates and the bridging intermediate is formed. Alternatively, we suggest that the pathway may proceed similarly with the sulfinate group acting as the base. Ultimately, both pathways follow similar chemistry and lead to the same bridging intermediate.

In order to confirm that these are viable pathways, these pathways must be explored through the same computational approaches taken throughout this thesis. These pathways would hopefully lead to a feasible pathway for the bridging intermediate formation.

6.2 References

(1) Heidari-Torkabadi, H.; Bethel, C. R.; Ding, Z.; Pusztai-Carey, M.; Bonnet, R.; Bonomo, R. A.; Carey, P. R. "Mind the Gap": Raman Evidence for Rapid Inactivation of CTX-M-9 beta-Lactamase Using Mechanism-Based Inhibitors that Bridge the Active Site. *J. Am. Chem. Soc.* **2015**, *137*, 12760.

(2) Aziz, J.; Messaoudi, S.; Alami, M.; Hamze, A. Sulfinate derivatives: dual and versatile partners in organic synthesis. *Organic & Biomolecular Chemistry* **2014**, *12*, 9743.

Vita Auctoris

Name:	Travis DeWolfe
Place of Birth:	Windsor, Ontario
Year of Birth:	1987
Education:	University of Windsor, B.Sc., Windsor, ON, 2015
	University of Windsor, M.Sc., Windsor, ON, 2017